Available online at www.sciencedirect.com
SCIENCE DIRECT®
ELSEVIER
Nuclear Physics A 756 (2005) 249–307
NUCLEAR PHYSICS A

Nuclear structure of ^{127}Te studied with (n, γ) and $(\vec{d}, p)$ reactions and interpreted with IBFM and QPM

J. Honzátko [a], V. Bondarenko [c], I. Tomandl [a,*], T. von Egidy [b], H.-F. Wirth [b], D. Bucurescu [d], V.Yu. Ponomarev [e,f], N. Mărginean [d], R. Hertenberger [g], Y. Eisermann [g], G. Graw [g], L. Rubáček [h]

[a] *Nuclear Physics Institute, 250 68 Řež, Czech Republic*
[b] *Physik-Department, Technische Universität München, D-85748 Garching, Germany*
[c] *Institute of Solid State Physics, University of Latvia, LV-1063 Riga, Latvia*
[d] *Horia Hulubei Institute of Physics and Nuclear Engineering, 76900 Bucharest, Romania*
[e] *Joint Institute for Nuclear Research, Dubna 141980, Russia*
[f] *Institut für Kernphysik, Technische Universität Darmstadt, D-64289 Darmstadt, Germany*
[g] *Department für Physik, Ludwig-Maximilians-Universität München, D-85748 Garching, Germany*
[h] *Faculty of Nuclear Science and Physical Engineering, Czech Technical University, 115 19 Prague, Czech Republic*

Received 13 December 2004; received in revised form 7 March 2005; accepted 24 March 2005

Available online 15 April 2005

Abstract

The nuclear structure of ^{127}Te has been investigated with the ^{126}Te$(n, \gamma\gamma)^{127}$Te reaction using thermal neutrons and with the ^{126}Te$(\vec{d}, p)^{127}$Te reaction at $E_d = 20$ MeV. About 190 levels were identified in a region to 4.1 MeV excitation energy, in most cases including spin, parity and γ-decay. The γ-decay scheme after neutron capture is essentially complete containing about 100% of the population of the $11/2^-$ isomer and of the ground state. The thermal neutron capture cross section and isomer production of the $11/2^-$ state at 88.3 keV were determined to be 0.44(6) b and 0.069(10) b, respectively. The neutron binding energy was determined to be 6287.6(1) keV. A significant number of the (d, p) angular distributions of cross section and asymmetry are anomalous with respect to

* Corresponding author.
E-mail address: tomandl@ujf.cas.cz (I. Tomandl).

0375-9474/$ – see front matter
doi:10.1016/j.nuclphysa.2005.03.060

the distorted-wave Born-approximation calculations and could be accounted for by inelastic multi-step mechanisms. The observed strong correlation of the (d, p) and primary (n, γ) strengths gives evidence for the direct neutron capture process which is mainly responsible for the primary population of 16 levels. The experimental level scheme is compared with predictions of the interacting boson–fermion model and of the quasiparticle phonon model.

PACS: 21.10.-k; 21.10.Jx; 21.60.Ev; 27.60.+j

Keywords: NUCLEAR REACTIONS: ^{126}Te(n, γ), $E =$ thermal; measured E_γ, I_γ, $\gamma\gamma$-coincidence; ^{126}Te(d, p), $E = 20$ MeV, polarized d; measured particle spectra, $\sigma(\theta)$, asymmetry. ^{127}Te deduced levels, J^π, γ-branching ratios, cross sections, binding energy, DWBA, CCBA spectroscopic factors. IBFM and QPM calculation and comparison. Direct neutron capture. Enriched targets; Ge detectors; Q3D magnetic spectrograph

1. Introduction

The long chain of available Te isotopes provides a nice possibility for the detailed study of the properties of nuclei undergoing a transition from an almost closed shell structure (^{131}Te, $N = 79$) to structures that have increased deformation near mid-shell (^{119}Te, $N = 67$). Systematic changes in the level energies and gamma decay modes have been interpreted [1] as a smooth admixture of O(6) to the dominant U(5) structure in the frame of the interacting boson model. It has been also possible in past to analyze the energy spectra and spectroscopic factors of the odd-A Te nuclides by quasiparticle-phonon coupling [2]. The nuclides near the $A \cong 130$ mass region have been the focus of calculations [3] using the U(6/20) supersymmetry. The recognition of different structures in the odd-mass Te nuclei and its extension to the higher energies may help to assess the validity of various nuclear structure models. However, it requires almost complete experimental data including spins, parities, electromagnetic properties and spectroscopic strengths.

The present work is a part of our joint project in which detailed and systematic investigations of the Te nuclides have been carried out using light particle induced transfer and thermal neutron capture reactions: ^{119}Te [4], ^{121}Te [1], ^{122}Te [5], ^{123}Te [6], ^{124}Te [7,8], ^{125}Te [9], ^{126}Te [10,11], ^{129}Te [12] and ^{131}Te [13]. In the present work we have studied the structure of the ^{127}Te nucleus with (d, p) and (n, γ) reactions. The application of polarized deuterons allowed to avoid many ambiguities of the previous spin-parity determination. The measurement of $\gamma\gamma$-coincidences enabled us to place most of transitions in the decay scheme. Thus a reliable set of data can be obtained for the comparison with different theoretical predictions. As in the case of our previous and current studies we use also the interacting boson–fermion model (IBFM-1) [14] and for the description of the high-lying states the quasiparticle phonon model (QPM) [15].

In earlier investigations compiled in Ref. [16] the energy levels have been studied by means of stripping [17,18] and pick-up [19] reactions and several beta decay works.

2. Experimental procedures and results

2.1. Thermal neutron capture studies

The single $^{126}\mathrm{Te}(n,\gamma)$ and $\gamma\gamma$-coincidence measurements were performed with two HPGe detectors installed at the light-water reactor LWR-15 at Řež near Prague. A 25% HPGe detector with a resolution of 1.95 at 1332 keV and 4.8 keV at 6 MeV and a 28% HPGe detector with about the same resolution were applied. The target material consisted of 413 mg metallic Te enriched in ^{126}Te to 98%. It was pressed to a disc of 8 mm diameter and was irradiated in a thermal neutron beam of about 10^6 n cm^{-2} s^{-1} from an external neutron guide. The experimental arrangement has been described in detail elsewhere [20].

The single γ-ray spectra were measured in two energy intervals (100–1500 keV and up to the binding energy). The energy calibration of the low energy portion of the γ-ray spectrum was performed in a separate run. This spectrum was obtained by parallel recording of γ-rays from neutron capture and from a radioactive source of ^{152}Eu. The energy calibration of the high energy portion of the spectra was made with well-known prominent background lines of $^{2}\mathrm{H}(n,\gamma)$ [21], $^{35}\mathrm{Cl}(n,\gamma)$ [22] and ^{60}Co [23]. Relative efficiencies of the HPGe detectors were determined using intensities from the $^{35}\mathrm{Cl}(n,\gamma)$ reaction [24] and ^{152}Eu [25]. The absolute intensity calibration of the ^{127}Te spectra was made using the activation line intensities of the daughter ^{127}I isotope [25]. Since the ground state of ^{127}Te is unstable to β-decay ($T_{1/2} = 9.4$ h) and because 1.19% of the disintegrations populate the 417.6 keV state in ^{127}I, it is possible to determine the absolute intensities quite readily. A close background line at 416.7 keV from the $^{115}\mathrm{In}(n,\gamma)$ reaction was taken into account in evaluation process. The measurement was performed after equilibrium of the ^{127g}Te decay was achieved. The isomer contribution from ^{127m}Te has been corrected taking into account the internal conversion factor. After subtraction of the background an absolute intensity of the 543 keV transition in ^{127}Te equal to 6.24 per 100 captured neutrons with a

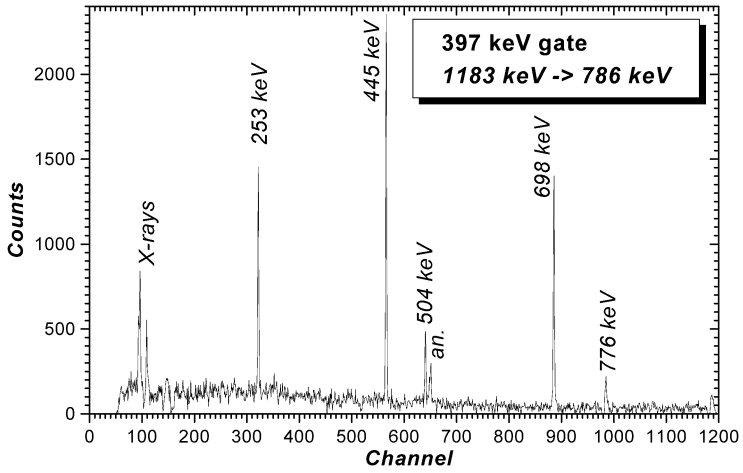

Fig. 1. The $\gamma\gamma$ coincidence spectrum of the 397 keV gate. The peaks are labelled with their energy.

relative statistical uncertainty of 8% was obtained. The systematic error was estimated to be 13%.

The coincidence data were recorded in an event-by-event mode for the run time of ≈ 500 hours. About 150 meaningful coincidence spectra were generated off-line. Combining results from evaluations of these coincidence spectra we were able to place about 500 γ transitions into the level scheme. An example of the coincidence spectrum is shown in Fig. 1. In addition to the large number of standard coincidence spectra we extracted 8 two-step cascade (TSC) spectra. The creation of these spectra is based on the application of the sum coincidence technique for semiconductor detectors [20,26,27].

The γ-ray energies observed in the single spectrum and in the $\gamma\gamma$-coincidences as well, their absolute intensities and their placements in the level scheme are given in Table 1. The gamma decay of the levels is given in Table 2.

Using the level scheme discussed later, the neutron binding energy was determined to be 6287.6(2) keV compared to 6287.8(4) keV in the mass tables [28]. Our value is based on the combination of many cascades connecting the capturing states with the ground state. Thanks averaging procedure the statistical error is very small, below 0.1 keV. Thus main uncertainty follow from the energy calibration in the region above 3 MeV.

2.2. The (d, p) studies

The ^{126}Te$(d, p)^{127}$Te measurements were performed at the Tandem Van de Graaff Accelerator of the Ludwig Maximilians University (LMU) and the Technical University of Munich (TUM). The target was made from metallic tellurium enriched to 98% (^{126}Te) deposited in vacuum on a carbon foil backing (about 5 μg/cm^2). We found few contaminating peaks in the spectra mainly attributed to the heaviest Te isotopes ($A = 129, 131$). The incoming polarized deuteron beam from a Lamb-shift negative-ion source [30] was accelerated to 20 MeV with the vector polarization typically of $\pm 60\%$. The outgoing protons were analyzed with the Q3D magnetic spectrograph [31] at 7 angles between 20° and 45°. The acceptance opening of the spectrograph was 6 msr. The momentum-separated products were detected by the 1.8 m long position sensitive proportional chamber [32] placed along the focal plane. The detector provided a good background suppression using particle identification via the energy-loss signal on the wires and the energy-rest signal produced by the particles stopped in a plastic scintillator. The energy range covered by the detector chamber for one magnetic setting of the Q3D was about 3.8 MeV. The position-sensitive detector allows the reconstruction of the focal plane which essentially improves the resolution depending of the position. The best resolution in the middle region of the detector obtained after the computer trace reconstruction procedure was 3.7 keV (FWHM) and a sample spectrum is shown in Fig. 2. The absolute cross sections were obtained from the beam intensity integrated in a Faraday cup. The currents during the experiment were in the order of 100 nA. For the absolute energy calibration we used the excitation energies of levels determined in the present (n, γ) studies which were identified also in the (d, p) spectra. This procedure gives an excellent accuracy for the low and medium energies where there are no problems with the identification of the levels in both processes. Difficulties

Table 1
List of observed γ transitions with their absolute intensities and their placement

Transition (keV)[a]	$I\ \frac{1}{100n}$	$\frac{\Delta I}{I}$ (%)	E_i (keV)	Transition (keV)	$I\ \frac{1}{100n}$	$\frac{\Delta I}{I}$ (%)	E_i (keV)
61.2(2)	–	–	61	546.8(3)	0.13	20	1309
139.3(7)	0.06	12	763	551.72(4)	1.38	2	1183
154.6(4)	0.06	33	786	558.6(4)	0.08	26	2338
170.7(4)	0.09	19	1354	561.79(2)	3.23	1	623
180.41(24)	0.18	10	–	567.6(3)	0.22	12	1354
183.6(3)	0.05	36	685	571.27(18)	0.26	19	1354
212.23(22)	0.20	8	685	573.06(12)	0.50	4	1075
237.3(4)	–	–	1806	575.7(4)	0.06	32	1758
239.4(8)	0.04	40	924	580.6(3)	0.11	21	2360
243.1(3)	0.07	32	2561	583.0(4)	0.14	27	924
252.73(5)	7.38	1	341	591.27(21)	0.25	8	1354
260.6(3)	0.16	12	763	596.05(12)	0.51	17	1379
280.8(4)	0.11	30	783	598.45(23)	0.06	18	2207
283.3(3)	–	–	2167	601.83(5)	0.63	25	1075
290.54(3)	3.12	1	631	604.11(24)	0.14	15	1077
289.40(22)	0.45	7	763	604.4(3)	0.17	26	1290
292.6(3)	0.09	20	924	608.5(3)	0.04	23	1293
292.7(4)	0.10	39	1075	611.2(4)	0.07	33	2300
309.4(4)	0.05	28	783	612.0(4)	0.06	27	2391
354.1(10)	0.34	32	2561	612.4(3)	0.11	22	1688
357.4(5)	0.09	27	1140	615.8(7)	0.13	2	1379
364.7(5)	0.10	22	2144	622.93(6)	6.45	2	623
387.3(4)	0.07	15	1462	637.94(22)	0.07	19	2246
391.8(3)	0.03	26	1077	638.32(5)	0.77	7	1140
397.00(3)	1.54	1	1183	638.9(3)	0.20	21	2190
403.2(7)	0.09	23	2593	646.6(4)	0.04	38	2254
411.99(4)	1.55	2	473	652.77(10)	0.35	12	1155
440.77(2)	4.56	1	502	655.9(5)	0.05	36	2010
445.26(3)	2.43	1	786	666.8(3)	0.07	25	1290
451.0(7)	0.17	25	924	667.0(3)	0.88	15	1140
452.22(25)	0.42	9	1075	681.32(20)	0.31	7	1155
454.9(3)	0.33	3	1140	684.96(5)	2.02	1	685
456.5(3)	0.04	24	2144	686.5(3)	0.34	9	1309
459.6(5)	0.04	31	2469	694.0(3)	0.22	23	1379
467.2(3)	0.12	31	2246	697.87(6)	2.23	2	786
473.29(7)	10.50	5	473	699.0(4)	0.05	27	1462
475.2(5)	0.08	20	2619	700.0(6)	0.04	39	1884
479.36(11)	0.16	37	2030	701.40(4)	2.34	2	763
493.5(4)	0.20	15	1568	703.1(4)	0.17	25	2254
501.93(1)	9.36	1	502	704.6(2)	0.34	17	1845
504.50(13)	0.25	13	1688	709.7(4)	0.22	18	2318
517.29(10)	0.97	4	1140	717.9(4)	0.20	20	2497
526.4(4)	0.08	29	1309	721.8(5)	0.47	22	783
527.23(17)	0.07	15	1290	722.60(20)	2.38	16	1354
530.6(3)	0.05	20	1293	729.9(4)	0.03	30	2338
535.90(13)	0.29	11	2144	730.83(12)	0.60	5	1354
538.6(4)	–	–	1462	743.9(3)	0.19	12	1429
539.0(3)	0.12	33	2318	751.46(22)	0.12	28	2360
543.20(1)	6.24	1	631	762.57(6)	5.59	2	763

(*continued on next page*)

Table 1 (*continued*)

Transition (keV)[a]	$I\ \frac{1}{100n}$	$\frac{\Delta I}{I}$ (%)	E_i (keV)	Transition (keV)	$I\ \frac{1}{100n}$	$\frac{\Delta I}{I}$ (%)	E_i (keV)
764.6(7)	0.03	41	1551	1043.4(10)	0.12	25	1806
775.9(4)	0.12	25	1959	1043.9(6)	0.08	32	2120
782.63(3)	3.72	1	783	1053.8(6)	0.19	13	1556
787.89(13)	0.30	10	1290	1055.8(7)	0.17	16	1688
792.7(5)	0.06	33	1976	1062.3(7)	0.30	16	2246
794.5(5)	0.07	37	1868	1062.9(3)	0.08	17	2469
806.7(3)	0.04	24	1492	1064.00(17)	0.44	42	1847
807.52(18)	0.34	15	1309	1064.1(6)	0.39	12	1688
813.37(24)	0.15	27	2593	1066.4(7)	0.19	17	2955
816.62(20)	0.43	6	1290	1075.0(3)	0.44	7	1075
819.92(8)	0.20	26	1293	1081.3(4)	0.06	25	1704
822.12(15)	0.73	5	1608	1083.8(3)	0.09	13	1847
826.7(3)	0.08	23	2010	1094.9(3)	0.23	31	1568
834.6(4)	0.08	23	2144	1097.71(19)	0.16	10	1884
835.80(21)	0.09	16	1309	1105.7(5)	0.03	30	1868
842.21(6)	1.38	2	1183	1115.9(3)	0.05	22	1878
846.4(5)	0.07	29	2030	1116.9(5)	0.06	27	2300
851.6(4)	0.09	23	1354	1118.4(2)	0.09	16	1804
852.9(4)	0.19	14	2207	1126.4(11)	0.09	33	1889
882.97(12)	0.13	29	1568	1131.0(5)	0.03	33	1815
885.6(7)	0.19	18	2773	1134.9(3)	0.33	9	2318
889.06(20)	0.08	45	2497	1138.9(5)	0.06	27	1612
892.3(6)	0.22	18	2246	1139.90(23)	0.37	17	1140
901.1(6)	0.19	14	1688	1147.44(11)	0.92	3	1779
904.0(5)	0.17	16	1406	1149.1(6)	0.06	35	2458
905.3(5)	0.04	29	1379	1154.5(5)	0.19	16	2338
911.1(5)	0.03	34	2519	1161.8(4)	0.04	26	1847
919.45(15)	0.10	15	1551	1164.5(2)	0.09	15	2773
924.0(3)	0.26	13	924	1172.98(19)	0.20	11	1959
932.2(5)	0.03	38	1406	1173.5(3)	0.19	24	1956
939.5(3)	0.35	6	2318	1175.7(5)	0.10	34	2360
941.9(6)	0.15	14	1704	1177.8(6)	0.27	21	2318
945.3(3)	0.07	16	2955	1187.2(8)	0.13	17	2593
952.9(7)	0.12	18	2561	1188.4(4)	0.16	32	2328
961.20(10)	0.14	23	2144	1193.0(6)	0.07	40	1976
964.0(8)	0.16	22	2318	1194.1(5)	0.20	18	1956
971.9(4)	0.08	22	1758	1207.4(4)	0.08	24	2561
976.80(8)	1.55	2	1608	1208.2(6)	0.05	26	2391
984.1(4)	0.32	11	2593	1209.73(12)	0.41	5	1551
989.1(6)	0.06	33	1462	1210.2(5)	0.07	26	1683
990.5(3)	0.19	28	1773	1215.5(5)	0.05	30	1847
992.9(3)	0.28	7	1779	1224.2(4)	0.08	24	1847
993.9(3)	0.12	47	2773	1225.24(23)	0.13	26	2913
996.5(3)	0.24	24	1779	1227.4(7)	0.07	40	2010
1009.3(6)	0.18	16	2318	1229.6(7)	0.16	15	1290
1010.2(4)	0.04	23	1773	1230.1(6)	0.04	28	1993
1013.80(6)	1.08	2	1075	1231.02(22)	0.15	12	1704
1023.3(5)	0.17	15	1806	1238.3(5)	0.05	31	1868
1024.0(4)	0.06	34	2207	1238.6(8)	0.14	29	2593
1028.7(4)	0.07	25	1815	1239.7(5)	0.06	31	2026

Table 1 (*continued*)

Transition (keV)[a]	$I\ \frac{1}{100n}$	$\frac{\Delta I}{I}$ (%)	E_i (keV)	Transition (keV)	$I\ \frac{1}{100n}$	$\frac{\Delta I}{I}$ (%)	E_i (keV)
1243.76(22)	0.15	13	2030	1398.7(3)	0.12	15	2030
1245.1(5)	0.06	32	1868	1403.6(9)	0.15	21	2190
1247.3(5)	0.03	32	2010	1404.9(4)	0.08	32	1878
1248.04(22)	0.45	7	1309	1409.0(9)	0.15	21	2593
1252.5(5)	0.07	25	1884	1416.9(4)	0.11	19	1758
1254.1(4)	0.10	19	1878	1416.9(2)	0.19	13	2102
1265.0(4)	0.09	31	2340	1420.3(13)	0.08	32	2207
1265.8(5)	0.06	33	2619	1424.10(11)	0.20	12	2207
1265.9(2)	0.58	5	1889	1425.20(14)	0.25	13	2049
1266.3(3)	0.14	29	2049	1438.7(6)	0.05	33	1779
1268.1(7)	0.11	29	1608	1442.2(4)	0.20	27	2225
1271.06(4)	1.64	7	1773	1443.9(2)	0.51	5	2207
1271.40(12)	0.18	14	1956	1454.4(4)	0.25	10	1956
1274.0(7)	0.19	17	2056	1458.0(5)	0.23	10	1959
1277.3(6)	0.08	32	1779	1461.2(2)	0.07	14	2244
1283.5(6)	0.06	20	2593	1462.30(22)	0.11	16	2225
1286.0(3)	0.06	18	2049	1473.1(4)	0.11	24	1976
1288.5(5)	0.19	36	2429	1483.37(25)	0.45	5	1956
1289.4(3)	0.49	5	1290	1486.2(3)	0.13	18	2109
1290.2(6)	0.05	23	1919	1490.5(12)	0.40	31	1993
1291.2(6)	0.05	42	1976	1502.6(3)	0.26	17	2856
1292.68(16)	0.36	11	1354	1507.6(4)	0.06	31	2690
1292.7(4)	0.07	23	1916	1508.1(3)	0.34	18	2010
1299.8(3)	0.13	20	1773	1515.2(4)	0.06	20	2278
1306.2(5)	–	–	3154	1515.5(3)	0.12	15	2138
1306.3(5)	0.06	35	1779	1519.40(25)	0.14	110	1993
1309.2(1)	1.25	2	1309	1528.26(18)	0.30	12	2030
1313.22(25)	0.23	18	2497	1533.8(7)	0.05	34	2157
1313.8(3)	0.06	31	2667	1536.72(25)	0.35	14	2010
1318.7(5)	0.21	13	–	1542.09(25)	0.22	25	2305
1323.1(6)	0.03	45	2932	1545.73(18)	0.33	18	2328
1328.6(6)	0.05	33	1959	1546.81(21)	0.20	8	2730
1332.31(8)	0.47	11	1806	1546.88(13)	0.44	10	2049
1333.18(7)	0.57	11	1956	1552.9(3)	0.33	14	2176
1344.65(11)	0.47	9	1847	1554.30(13)	0.48	9	2056
1344.9(4)	0.67	7	1406	1555.2(3)	0.09	23	2318
1346.6(3)	0.07	23	2955	1555.4(6)	0.09	39	2338
1357.3(4)	0.06	20	2120	1556.1(4)	0.11	21	2030
1358.6(4)	0.11	23	2144	1558.0(4)	0.18	22	2190
1370.0(9)	0.16	19	1993	1559.9(4)	0.07	41	2913
1371.2(3)	0.07	19	2056	1561.6(4)	0.10	37	2916
1373.8(4)	0.08	24	1847	1564.68(17)	0.16	13	2327
1375.95(15)	0.39	9	1878	1568.5(6)	0.21	33	1568
1377.98(25)	0.14	19	2561	1574.7(4)	0.23	27	2358
1378.42(14)	0.80	8	1379	1575.68(20)	0.18	19	2049
1386.35(25)	0.12	17	2010	1577.0(4)	0.24	20	2340
1386.6(10)	0.15	23	1889	1578.3(5)	0.12	33	2360
1394.1(5)	0.05	33	2469	1579.1(4)	0.09	23	1919
1394.2(2)	0.11	14	2157	1583.7(6)	0.06	31	2056
1394.5(5)	0.26	10	1868	1583.83(10)	0.55	6	2207

(*continued on next page*)

Table 1 (*continued*)

Transition (keV)[a]	$I\ \frac{1}{100n}$	$\frac{\Delta I}{I}$ (%)	E_i (keV)	Transition (keV)	$I\ \frac{1}{100n}$	$\frac{\Delta I}{I}$ (%)	E_i (keV)
1588.5(4)	0.14	29	2878	1836.1(7)	0.05	35	2458
1598.9(6)	0.09	32	2102	1840.6(3)	0.25	15	–
1601.5(4)	0.21	32	2225	1844.53(10)	0.63	16	2318
1605.6(5)	0.08	29	2391	1845.87(22)	0.18	11	2469
1607.29(12)	0.53	8	2109	1855.2(3)	0.15	15	2328
1623.7(5)	0.08	26	2932	1856.1(3)	0.24	13	2358
1624.5(6)	0.07	29	2254	1865.0(3)	0.20	18	2338
1625.3(5)	0.07	33	2979	1869.5(3)	0.19	17	2493
1626.3(3)	0.16	21	–	1877.88(24)	0.27	12	1878
1635.5(3)	0.38	17	2109	1885.1(5)	0.09	23	2358
1635.9(6)	0.09	29	2138	1888.1(3)	0.27	15	1889
1637.2(5)	0.11	32	3416	1888.3(4)	0.09	20	2519
1646.0(3)	0.11	19	2120	1895.4(6)	0.07	28	1956
1647.3(4)	0.18	24	2278	1936.7(3)	0.21	15	2438
1649.4(3)	–	–	3679	1948.6(5)	0.10	25	3132
1655.4(3)	0.22	26	2438	1948.72(7)	1.98	3	2010
1664.9(3)	0.16	18	2138	1948.8(6)	0.05	29	2712
1675.74(19)	0.13	13	2438	1956.6(4)	0.30	19	1956
1676.0(3)	0.22	21	2458	1966.9(5)	0.05	29	2730
1686.4(4)	0.20	20	2318	1966.96(8)	0.97	7	2469
1693.9(6)	0.06	29	2878	1969.6(5)	0.09	23	2593
1694.65(15)	0.47	8	2318	1984.8(3)	0.13	18	2458
1698.7(7)	0.03	44	2773	1987.3(6)	0.08	27	2773
1704.8(8)	0.73	17	2207	1991.5(6)	0.10	25	2493
1704.9(3)	0.11	21	2328	1992.75(21)	0.07	94	1993
1706.4(3)	2.17	5	2469	2009.9(6)	0.21	32	2010
1706.4(5)	0.08	26	2338	2044.5(5)	0.07	30	2667
1711.8(6)	0.07	38	1773	2058.05(22)	0.06	34	2690
1723.1(3)	0.20	14	2225	2058.85(12)	0.61	6	2120
1730.0(7)	0.05	47	2913	2061.0(5)	0.04	47	3866
1733.1(4)	0.10	24	2207	2067.1(7)	0.06	29	2690
1733.6(4)	0.10	23	2916	2077.2(3)	0.17	34	3764
1743.4(6)	0.04	30	2429	2080.9(3)	0.13	15	2554
1744.2(3)	0.22	18	2246	2082.95(9)	2.34	5	2144
1748.6(7)	0.12	30	2932	2090.67(20)	0.36	12	2593
1751.8(4)	0.14	20	2254	2099.90(20)	0.34	11	–
1752.0(4)	0.09	22	2225	2115.6(7)	0.14	39	3255
1760.2(4)	0.10	18	2391	2115.8(6)	0.08	41	2878
1770.6(5)	0.08	25	2244	2117.28(20)	0.58	6	2619
1770.7(7)	0.22	35	2955	2122.07(18)	0.38	9	2905
1773.1(4)	0.38	21	1773	2136.8(6)	0.21	24	2138
1776.6(5)	0.54	8	2278	2145.57(1)	9.23	1	2207
1780.6(4)	0.36	18	2254	2150.2(6)	0.08	32	2773
1801.9(9)	0.09	30	2305	2151.0(5)	0.08	41	2913
1805.2(6)	0.08	26	2593	2156.7(4)	0.28	18	–
1806.52(17)	0.39	9	2429	2175.4(5)	0.31	21	2176
1816.14(16)	0.32	9	2318	2187.5(7)	0.09	31	2690
1827.67(20)	0.35	10	1889	2192.5(5)	0.13	27	2955
1831.1(3)	0.30	14	1919	2206.77(4)	2.40	2	2207
1835.6(7)	0.08	38	2338	2209.0(5)	0.11	25	3392

Table 1 (*continued*)

Transition (keV)[a]	$I\ \frac{1}{100n}$	$\frac{\Delta I}{I}$ (%)	E_i (keV)	Transition (keV)	$I\ \frac{1}{100n}$	$\frac{\Delta I}{I}$ (%)	E_i (keV)
2217.2(5)	0.09	24	2690	2529.8(7)	0.14	37	3884
2230.4(3)	0.40	19	6288	2533.2(4)	0.27	14	2593
2233.4(6)	0.17	24	3416	2557.92(8)	1.21	3	2619
2250.9(3)	–	–	6288	2561.8(3)	0.23	13	2561
2267.1(6)	0.13	27	–	2568.7(6)	0.15	24	3922
2271.0(4)	0.14	17	2773	2580.8(8)	0.08	39	3765
2271.5(6)	0.07	26	2905	2592.5(3)	0.40	11	2593
2278.45(19)	0.43	9	2340	2606.9(8)	0.03	36	2667
2289.4(7)	0.04	48	2913	2608.68(15)	0.59	6	6288
2289.4(6)	0.08	26	2763	2619.2(3)	0.26	15	2619
2292.9(4)	0.23	18	2916	2624.2(6)	0.22	36	3765
2299.4(7)	0.09	34	2773	2629.2(4)	0.22	21	2690
2309.2(5)	0.09	23	2932	2630.7(8)	0.05	3	3392
2313.93(25)	0.39	10	6288	2653.2(6)	0.16	25	3416
2318.1(6)	0.14	25	2318	2664.6(6)	0.08	30	3286
2331.5(6)	0.08	25	2955	2667.13(23)	0.32	15	2667
2338.6(4)	0.24	30	2338	2668.9(4)	0.34	14	2730
2339.5(3)	0.31	12	2340	2669.9(3)	0.09	38	3853
2348.8(7)	0.07	33	3132	2680.1(6)	0.07	26	3154
2359.37(22)	0.24	19	2360	2683.1(9)	0.07	41	3866
2363.3(5)	0.10	25	2994	2690.5(6)	0.10	30	2690
2365.29(9)	0.95	4	6288	2700.5(3)	0.45	10	2700
2371.31(17)	0.48	8	–	2711.7(4)	0.10	42	2773
2371.4(8)	0.10	41	3154	2720.5(3)	0.33	14	6288
2376.4(4)	0.11	37	2878	2729.5(4)	0.24	19	2730
2377.24(14)	0.26	21	2438	2742.16(12)	0.68	5	6288
2404.0(5)	0.13	25	2905	2759.0(3)	0.30	16	2759
2404.00(20)	0.48	8	6288	2762.2(7)	0.10	38	2763
2404.9(6)	0.07	43	2878	2769.6(6)	0.11	45	3392
2407.85(9)	0.83	4	2469	2773.7(5)	0.07	43	2773
2422.04(16)	0.52	7	6288	2781.8(5)	0.11	22	3255
2428.4(3)	0.28	12	2429	2773.7(5)	0.07	43	2773
2430.1(7)	0.08	29	2905	2781.8(5)	0.11	22	3255
2434.73(12)	0.66	7	6288	2793.3(5)	0.16	15	3416
2435.47(16)	0.91	25	2497	2795.4(3)	0.41	30	2856
2438.4(3)	0.06	22	2438	2804.3(8)	0.04	36	3567
2442.1(5)	0.15	29	2916	2816.73(25)	0.20	41	2878
2451.5(4)	0.32	16	6288	2851.7(6)	0.09	4	2913
2454.5(12)	0.08	43	2955	2868.5(3)	0.31	13	–
2458.6(7)	0.08	33	2932	2871.5(4)	0.35	12	6288
2468.97(5)	2.36	2	2469	2873.4(3)	0.22	15	3375
2481.4(3)	0.14	18	2955	2877.7(8)	0.04	49	2878
2484.8(5)	0.15	24	–	2896.00(17)	0.54	7	6288
2491.7(4)	0.09	28	3255	2912.7(5)	0.16	21	3416
2492.1(5)	0.15	26	2994	2916.45(25)	0.36	10	2916
2496.4(6)	–	–	3679	2918.6(4)	0.17	19	3392
2500.2(6)	0.11	30	2561	2943.3(6)	0.08	32	3567
2505.5(5)	0.08	25	2979	2943.6(8)	0.11	23	3416
2523.09(16)	0.82	6	6288	2955.2(9)	0.13	39	2955
2523.4(6)	0.06	33	3287	2956.1(7)	0.06	43	3719

(*continued on next page*)

Table 1 (*continued*)

Transition (keV)[a]	$I\ \frac{1}{100n}$	$\frac{\Delta I}{I}$ (%)	E_i (keV)	Transition (keV)	$I\ \frac{1}{100n}$	$\frac{\Delta I}{I}$ (%)	E_i (keV)
2969.3(4)	0.27	19	–	3790.63(21)	0.63	7	6288
3093.8(6)	0.18	24	3595	3804.9(5)	0.03	58	3866
3093.9(7)	0.08	1	3154	3818.66(3)	6.37	1	6288
3094.9(5)	0.25	15	3567	3821.8(4)	0.41	24	3884
3099.0(6)	0.07	30	3572	3835.9(6)	0.23	27	3836
3129.3(5)	0.26	18	–	3849.18(25)	0.53	10	6288
3154.5(7)	0.12	25	3154	3857.9(4)	0.43	13	6288
3209.3(5)	0.22	27	–	3860.90(23)	0.27	22	3922
3218.5(7)	0.06	51	3719	3883.9(3)	0.57	23	3884
3235.2(8)	0.07	29	3866	3912.7(5)	0.27	52	3974
3332.90(14)	0.86	6	6288	3922.7(6)	0.06	29	3922
3334.6(6)	0.13	34	3836	3928.7(6)	0.23	20	6288
3350.2(6)	0.13	48	3853	3949.5(3)	0.31	14	6288
3355.8(4)	0.26	18	6288	3954.5(9)	0.08	4	3954
3363.3(4)	0.07	46	3866	3959.1(6)	0.33	32	6288
3372.08(23)	0.92	8	6288	3969.58(6)	2.39	2	6288
3374.2(6)	0.43	16	6288	3974.3(8)	0.13	54	3974
3380.1(5)	0.09	45	3853	3975.3(4)	–	–	4036
3382.3(5)	0.48	32	6288	3996.4(4)	0.12	42	4057
3392.2(9)	0.05	49	3392	4036.2(8)	–	–	4036
3397.0(8)	0.13	37	–	4041.62(25)	0.55	10	6288
3409.5(5)	0.13	20	3884	4080.75(3)	13.00	1	6288
3409.6(3)	0.41	11	6288	4112.2(5)	0.27	17	6288
3431.5(6)	0.19	23	6288	4131.1(10)	–	–	6288
3480.6(6)	0.02	25	3954	4143.42(7)	2.34	2	6288
3484.4(3)	0.36	12	3545	4149.6(5)	0.25	42	6288
3506.6(4)	0.11	41	3567	4167.2(3)	0.21	20	6288
3514.55(19)	0.57	9	6288	4178.9(3)	0.31	13	6288
3524.2(6)	0.16	8	6288	4277.70(7)	2.15	2	6288
3528.4(5)	0.42	16	6288	4287.6(6)	0.17	35	–
3545.5(3)	0.46	12	3545	4295.0(3)	0.45	11	6288
3557.6(3)	0.59	13	6288	4331.1(3)	0.44	11	6288
3567.6(5)	0.10	46	3567	4399.0(4)	0.39	12	6288
3584.0(5)	0.08	49	4057	4410.2(9)	–	–	6288
3586.5(4)	0.18	21	6288	4419.9(7)	0.29	66	6288
3597.6(5)	0.21	21	6288	4482.2(6)	0.23	21	6288
3617.3(11)	–	–	3679	4514.08(19)	0.85	6	6288
3620.50(21)	0.60	8	6288	4600.7(7)	–	–	6288
3658.9(7)	0.06	51	3719	4933.86(13)	1.84	7	6288
3668.19(9)	1.47	3	6288	4977.8(3)	0.22	27	6288
3679.0(6)	–	–	3679	5212.2(7)	0.19	27	6288
3694.76(9)	1.43	4	6288	5663.95(20)	0.98	5	6288
3704.1(9)	0.25	29	3765	5785.3(3)	0.87	8	6288
3718.9(9)	0.05	52	3719	5813.95(21)	0.48	12	6288
3726.23(24)	0.42	9	6288	6226.5(5)	0.76	14	6288
3750.1(4)	0.30	16	–	6287.15(9)	2.75	3	6288
3776.3(8)	0.11	30	3836				

[a] Only statistical errors are given. Systematic errors due to the energy calibration procedure are 0.1 keV for $E_\gamma < 3$ MeV and 0.2 keV for $E_\gamma > 3$ MeV.

Table 2
Gamma decay of the levels in ^{127}Te from the (n, γ) reaction. Gamma energies E_γ are recoil corrected

E_i (keV)	Spin	E_γ (keV)	I_γ (%)	E_f (keV)	Spin
0.00(0)	$3/2^+$				
61.17(1)	$1/2^+$				
		61.2	–	0.0	$3/2^+$
88.20(5)	$11/2^-$				
340.88(5)	$9/2^-$				
		252.7	7.38	88.2	$11/2^-$
473.21(3)	$5/2^+$				
		473.3	10.50	0.0	$3/2^+$
		412.0	1.55	61.2	$1/2^+$
501.93(1)	$3/2^+$				
		501.9	9.36	0.0	$3/2^+$
		440.8	4.56	61.2	$1/2^+$
622.98(2)	$1/2^+$				
		622.9	6.45	0.0	$3/2^+$
		561.8	3.23	61.2	$1/2^+$
631.41(5)	$7/2^-$				
		543.2	6.24	88.2	$11/2^-$
		290.5	3.12	340.9	$9/2^-$
684.99(5)	$7/2^+$				
		685.0	2.02	0.0	$3/2^+$
		212.2	0.20	473.2	$5/2^+$
		183.7	0.05	501.9	$3/2^+$
762.57(3)	$3/2^+$				
		762.6	5.59	0.0	$3/2^+$
		701.4	2.34	61.2	$1/2^+$
		289.4	0.45	473.2	$5/2^+$
		260.6	0.16	501.9	$3/2^+$
782.63(3)	$5/2^+$				
		782.6	3.72	0.0	$3/2^+$
		721.8	0.47	61.2	$1/2^+$
		309.4	0.05	473.2	$5/2^+$
		280.8	0.11	501.9	$3/2^+$
		139.3	0.06	623.0	$1/2^+$
786.12(5)	$7/2^-$				
		697.9	2.23	88.2	$11/2^-$
		445.3	2.43	340.9	$9/2^-$
		154.6	0.06	631.4	$7/2^-$
923.90(16)	$7/2^+$				
		924.0	0.26	0.0	$3/2^+$
		583.0	0.14	340.9	$9/2^-$
		451.0	0.17	473.2	$5/2^+$
		292.6	0.09	631.4	$7/2^-$
		239.4	0.04	685.0	$7/2^+$
1074.98(5)	$3/2^+$				
		1075.0	0.44	0.0	$3/2^+$
		1013.8	1.08	61.2	$1/2^+$
		601.8	0.63	473.2	$5/2^+$
		573.1	0.50	501.9	$3/2^+$
		452.2	0.42	623.0	$1/2^+$

(*continued on next page*)

Table 2 (*continued*)

E_i (keV)	Spin	E_γ (keV)	I_γ (%)	E_f (keV)	Spin
		292.7	0.10	782.6	$5/2^+$
1077.11(22)	$5/2^+, 9/2^+$				
		604.1	0.14	473.2	$5/2^+$
		391.8	0.03	685.0	$7/2^+$
1140.23(4)	$5/2^+$				
		1139.9	0.37	0.0	$3/2^+$
		667.0	0.88	473.2	$5/2^+$
		638.3	0.77	501.9	$3/2^+$
		517.3	0.97	623.0	$1/2^+$
		455.0	0.33	685.0	$7/2^+$
		357.4	0.09	782.6	$5/2^+$
1154.67(9)	$5/2, 7/2^+$				
		681.3	0.31	473.2	$5/2^+$
		652.8	0.35	501.9	$3/2^+$
1183.12(5)	$5/2^-$				
		842.2	1.38	340.9	$9/2^-$
		551.7	1.38	631.4	$7/2^-$
		397.0	1.54	786.1	$7/2^-$
1289.72(8)	$5/2^+$				
		1289.4	0.49	0.0	$3/2^+$
		1229.6	0.16	61.2	$1/2^+$
		816.6	0.43	473.2	$5/2^+$
		787.9	0.30	501.9	$3/2^+$
		666.8	0.07	623.0	$1/2^+$
		604.4	0.17	685.0	$7/2^+$
		527.2	0.07	762.6	$3/2^+$
1293.15(8)	$3/2^+, 5/2, 7/2^+$				
		819.9	0.20	473.2	$5/2^+$
		608.5	0.04	685.0	$7/2^+$
		530.6	0.05	762.6	$3/2^+$
1309.27(8)	$3/2^+$				
		1309.2	1.25	0.0	$3/2^+$
		1248.0	0.45	61.2	$1/2^+$
		835.8	0.09	473.2	$5/2^+$
		807.5	0.34	501.9	$3/2^+$
		686.5	0.34	623.0	$1/2^+$
		546.9	0.13	762.6	$3/2^+$
		526.4	0.08	782.6	$5/2^+$
1353.78(6)	$3/2^-$				
		1292.7	0.36	61.2	$1/2^+$
		851.6	0.09	501.9	$3/2^+$
		730.8	0.60	623.0	$1/2^+$
		722.6	2.38	631.4	$7/2^-$
		591.3	0.25	762.6	$3/2^+$
		571.3	0.26	782.6	$5/2^+$
		567.6	0.22	786.1	$7/2^-$
		170.7	0.09	1183.1	$5/2^-$
1378.59(8)	$5/2^+$				
		1378.4	0.80	0.0	$3/2^+$
		905.3	0.04	473.2	$5/2^+$

Table 2 (*continued*)

E_i (keV)	Spin	E_γ (keV)	I_γ (%)	E_f (keV)	Spin
		694.0	0.22	685.0	$7/2^+$
		615.8	0.13	762.6	$3/2^+$
		596.1	0.51	782.6	$5/2^+$
1405.88(20)	$1/2^+$				
		1344.9	0.67	61.2	$1/2^+$
		932.3	0.03	473.2	$5/2^+$
		904.0	0.17	501.9	$3/2^+$
1429.0(3)	$7/2^+$				
		744.0	0.19	685.0	$7/2^+$
1462.14(22)	$3/2^+, 5/2, 7/2^+$				
		989.1	0.06	473.2	$5/2^+$
		699.0	0.05	762.6	$5/2^+$
		387.3	0.07	1075.0	$3/2^+$
1491.7(3)	$(7/2^+)$				
		806.7	0.04	685.0	$7/2^+$
1550.64(10)	$(7/2^-, 5/2^-)$				
		1209.7	0.41	340.9	$9/2^-$
		919.5	0.10	631.4	$7/2^-$
		764.6	0.03	786.1	$7/2^-$
1555.7(6)	$5/2^+$				
		1053.8	0.19	501.9	$3/2^+$
1568.05(10)	$5/2^+$				
		1568.5	0.21	0.0	$3/2^+$
		1094.9	0.23	473.2	$5/2^+$
		883.0	0.13	685.0	$7/2^+$
		493.5	0.20	1075.0	$3/2^+$
1608.19(6)	$(5/2^-)$				
		1268.1	0.11	340.9	$9/2^-$
		976.8	1.55	631.4	$7/2^-$
		822.1	0.73	786.1	$7/2^-$
1612.1(5)	$(7/2^+)$				
		1138.9	0.06	473.2	$5/2^+$
1683.4(4)	$(5/2^+)$				
		1210.2	0.06	473.2	$5/2^+$
1687.59(11)	$3/2^-$				
		1064.1	0.39	623.0	$1/2^+$
		1055.8	0.17	631.4	$7/2^-$
		901.1	0.19	786.1	$7/2^-$
		612.4	0.11	1075.0	$3/2^+$
		504.5	0.25	1183.1	$5/2^-$
1704.22(8)	$3/2^+, 5/2^+$				
		1231.0	0.15	473.2	$5/2^+$
		1081.3	0.06	623.0	$1/2^+$
		941.9	0.15	762.6	$3/2^+$
1758.4(3)	$7/2^-$				
		1416.9	0.11	340.9	$9/2^-$
		971.9	0.08	786.2	$7/2^-$
		575.7	0.06	1183.1	$5/2^-$
1773.02(4)	$3/2^+$				
		1773.1	0.38	0.0	$3/2^+$

(*continued on next page*)

Table 2 (*continued*)

E_i (keV)	Spin	E_γ (keV)	I_γ (%)	E_f (keV)	Spin
		1711.8	0.07	61.2	$1/2^+$
		1299.8	0.13	473.2	$5/2^+$
		1271.1	1.64	501.9	$3/2^+$
		1010.2	0.04	762.6	$3/2^+$
		990.5	0.19	782.6	$5/2^+$
1778.99(8)	$5/2^-$				
		1438.7	0.05	340.9	$9/2^-$
		1306.3	0.06	473.2	$5/2^+$
		1277.3	0.08	501.9	$3/2^+$
		1147.4	0.92	631.4	$7/2^-$
		996.5	0.24	782.6	$5/2^+$
		992.9	0.28	786.1	$7/2^-$
1803.41(20)	$7/2^+$				
		1118.4	0.09	685.0	$7/2^+$
1805.51(8)	$1/2^+, 3/2$				
		1332.3	0.47	473.2	$5/2^+$
		1043.4	0.12	762.6	$3/2^+$
		1023.3	0.17	782.6	$5/2^+$
		237.3	–	1568.0	$5/2^+$
1815.3(4)	$7/2^-$				
		1131.0	0.03	685.0	$7/2^+$
		1028.7	0.07	786.2	$7/2^-$
1844.82(20)	$5/2^-$				
		704.6	0.34	1140.2	$5/2^+$
1846.7(8)	$3/2^+, 5/2^+$				
		1373.8	0.08	473.2	$5/2^+$
		1344.7	0.47	501.9	$3/2^+$
		1224.2	0.08	623.0	$1/2^+$
		1215.5	0.05	631.4	$7/2^-$
		1161.9	0.04	685.0	$7/2^+$
		1083.8	0.09	762.6	$3/2^+$
		1064.0	0.44	782.6	$5/2^+$
1868.2(2)	$1/2^+, 3/2, 5/2^+$				
		1394.9	0.26	473.2	$5/2^+$
		1245.1	0.06	623.0	$1/2^+$
		1238.3	0.05	631.4	$7/2^-$
		1105.8	0.03	762.6	$3/2^+$
		794.5	0.07	1075.0	$3/2^+$
1877.88(14)	$1/2^+, 3/2, 5/2^+$				
		1877.9	0.27	0.0	$3/2^+$
		1405.0	0.08	473.2	$5/2^+$
		1376.0	0.39	501.9	$3/2^+$
		1254.1	0.10	623.0	$1/2^+$
		1115.9	0.05	762.6	$3/2^+$
1883.79(19)	$(5/2^-)$				
		1252.5	0.07	631.4	$7/2^-$
		1097.7	0.16	786.1	$7/2^-$
		700.1	0.04	1183.1	$5/2^-$
1888.61(12)	$1/2^+$				
		1888.1	0.27	0.0	$3/2^+$

Table 2 (*continued*)

E_i (keV)	Spin	E_γ (keV)	I_γ (%)	E_f (keV)	Spin
		1827.7	0.35	61.2	$1/2^+$
		1386.6	0.15	501.9	$3/2^+$
		1265.9	0.58	623.0	$1/2^+$
		1126.4	0.09	762.6	$3/2^+$
1916.0(4)	$(3/2^+)$				
		1292.7	0.07	623.0	$1/2^+$
1919.3(3)	$7/2^-$				
		1290.2	0.05	631.4	$7/2^-$
		1579.1	0.09	340.9	$9/2^-$
		1831.1	0.30	88.2	$11/2^-$
1956.26(6)	$3/2^+$				
		1956.6	0.30	0.0	$3/2^+$
		1895.4	0.07	61.2	$1/2^+$
		1483.4	0.45	473.2	$5/2^+$
		1454.4	0.25	501.9	$3/2^+$
		1333.2	0.57	623.0	$1/2^+$
		1271.4	0.18	685.0	$7/2^+$
		1194.1	0.20	762.6	$3/2^+$
		1173.5	0.19	782.6	$5/2^+$
1959.22(18)	$(3/2^-)$				
		1458.0	0.23	501.9	$3/2^+$
		1328.6	0.05	631.4	$7/2^-$
		1173.0	0.20	786.1	$7/2^-$
		775.9	0.12	1183.1	$5/2^-$
1975.5(3)	$(5/2^+)$, 7/2				
		1473.2	0.11	501.9	$3/2^+$
		1291.2	0.05	685.0	$7/2^+$
		1193.0	0.07	782.6	$5/2^+$
		792.7	0.06	1183.1	$5/2^-$
1992.68(14)	3/2, $(1/2^+)$				
		1992.8	0.07	0.0	$3/2^+$
		1519.4	0.14	473.2	$5/2^+$
		1490.5	0.40	501.9	$3/2^+$
		1370.0	0.16	623.0	$1/2^+$
		1230.1	0.04	762.6	$3/2^+$
2009.83(5)	$3/2^-$				
		2009.9	0.21	0.0	$3/2^+$
		1948.7	1.98	61.2	$1/2^+$
		1536.7	0.35	473.2	$5/2^+$
		1508.1	0.34	501.9	$3/2^+$
		1386.4	0.12	623.0	$1/2^+$
		1247.4	0.03	762.6	$3/2^+$
		1227.4	0.07	782.6	$5/2^+$
		826.7	0.08	1183.1	$5/2^-$
		655.9	0.05	1353.8	$3/2^-$
2025.9(5)	$7/2^-$				
		1239.7	0.06	786.1	$7/2^-$
2030.00(10)	$3/2^-$, 5/2, $7/2^+$				
		1556.1	0.11	473.2	$5/2^+$
		1528.3	0.30	501.9	$3/2^+$

(*continued on next page*)

Table 2 (*continued*)

E_i (keV)	Spin	E_γ (keV)	I_γ (%)	E_f (keV)	Spin
		1398.7	0.12	631.4	$7/2^-$
		1243.8	0.15	786.1	$7/2^-$
		846.4	0.07	1183.1	$5/2^-$
		479.4	0.16	1550.6	$7/2^-(5/2^-)$
2048.61(14)	$1/2^+, 3/2, 5/2^+$				
		1575.7	0.18	473.2	$5/2^+$
		1546.9	0.44	501.9	$3/2^+$
		1425.2	0.25	623.0	$1/2^+$
		1286.0	0.06	762.6	$3/2^+$
		1266.3	0.14	782.6	$5/2^+$
2056.27(11)	$3/2^+, 5/2, 7/2^+$				
		1583.8	0.06	473.2	$5/2^+$
		1554.3	0.48	501.9	$3/2^+$
		1371.2	0.07	685.0	$7/2^+$
		1274.0	0.19	782.6	$5/2^+$
2101.8(3)					
		1598.9	0.09	501.9	$3/2^+$
		1416.9	0.09	685.0	$7/2^+$
2109.12(12)	$1/2^+, 3/2, 5/2^+$				
		1635.5	0.38	473.2	$5/2^+$
		1607.3	0.53	501.9	$3/2^+$
		1486.2	0.13	623.0	$1/2^+$
2119.96(15)	$1/2^+$				
		2058.9	0.61	61.2	$1/2^+$
		1646.0	0.11	473.2	$5/2^+$
		1357.3	0.06	762.6	$3/2^+$
		1043.9	0.08	1075.0	$3/2^+$
2138.11(22)	$1/2^+, 3/2$				
		2136.8	0.21	0.0	$3/2^+$
		1665.0	0.16	473.2	$5/2^+$
		1636.0	0.09	501.9	$3/2^+$
		1515.5	0.12	623.0	$1/2^+$
2144.15(5)	$3/2^-$				
		2083.0	2.34	61.2	$1/2^+$
		1358.6	0.11	786.1	$7/2^-$
		961.2	0.14	1183.1	$5/2^-$
		834.6	0.08	1309.2	$3/2^+$
		535.9	0.29	1608.2	$(5/2^-)$
		456.5	0.04	1687.6	$3/2^-$
		364.7	0.10	1779.0	$5/2^-$
2156.8(2)	$1/2, 3/2, 5/2^+$				
		1533.8	0.05	623.0	$1/2^+$
		1394.2	0.11	762.6	$5/2^+$
2167.1(3)	$7/2^-$				
		283.3	–	1883.8	$(5/2^-)$
2175.67(21)	$(3/2^+)$				
		2175.4	0.31	0.0	$3/2^+$
		1552.9	0.33	623.0	$1/2^+$
2189.53(23)	$3/2^-, 5/2, 7/2^-$				
		1558.1	0.18	631.4	$7/2^-$

Table 2 (*continued*)

E_i (keV)	Spin	E_γ (keV)	I_γ (%)	E_f (keV)	Spin
		1403.6	0.15	786.1	$7/2^-$
		638.9	0.20	1550.6	$7/2^-(5/2^-)$
2206.76(1)	$3/2^-$				
		2206.8	2.40	0.0	$3/2^+$
		2145.6	9.23	61.2	$1/2^+$
		1733.1	0.10	473.2	$5/2^+$
		1704.8	0.73	501.9	$3/2^+$
		1583.8	0.55	623.0	$1/2^+$
		1443.9	0.51	762.6	$3/2^+$
		1424.1	0.20	782.6	$5/2^+$
		1420.3	0.08	786.1	$7/2^-$
		1024.0	0.06	1183.1	$5/2^-$
		852.9	0.19	1353.8	$3/2^-$
		598.5	0.06	1608.2	$(5/2^-)$
2224.88(14)	$1/2^+$, 3/2, $5/2^+$				
		1752.0	0.09	473.2	$5/2^+$
		1723.1	0.20	501.9	$3/2^+$
		1601.5	0.21	623.0	$1/2^+$
		1462.3	0.11	762.6	$3/2^+$
		1442.2	0.20	782.6	$5/2^+$
2243.6(4)	$(7/2^+)$				
		1770.6	0.08	473.2	$5/2^+$
		1461.2	0.07	782.6	$5/2^+$
2246.07(13)	$3/2^-$				
		1744.2	0.22	501.9	$3/2^+$
		1062.3	0.30	1183.1	$5/2^-$
		892.3	0.22	1353.8	$3/2^-$
		637.9	0.07	1608.2	$(5/2^-)$
		467.2	0.12	1779.0	$5/2^-$
2254.12(20)	5/2, (7/2)				
		1780.7	0.36	473.2	$5/2^+$
		1751.9	0.14	501.9	$3/2^+$
		703.2	0.17	1550.6	$7/2^-(5/2^-)$
		646.6	0.04	1608.2	$(5/2^-)$
2278.32(25)	$(5/2^-)$				
		1776.6	0.54	501.9	$3/2^+$
		1647.3	0.18	631.4	$7/2^-$
		1515.2	0.06	762.6	$3/2^+$
2300.1(5)	$5/2^-$				
		1117.0	0.06	1183.1	$5/2^-$
		611.2	0.07	1687.6	$3/2^-$
2304.7(3)					
		1801.9	0.09	501.9	$3/2^+$
		1542.1	0.22	762.6	$5/2^+$
2317.90(5)	$3/2^-$				
		2318.1	0.14	0.0	$3/2^+$
		1844.5	0.63	473.2	$5/2^+$
		1816.2	0.32	501.9	$3/2^+$
		1694.7	0.47	623.0	$1/2^+$
		1686.4	0.20	631.4	$7/2^-$

(*continued on next page*)

Table 2 (*continued*)

E_i (keV)	Spin	E_γ (keV)	I_γ (%)	E_f (keV)	Spin
		1555.2	0.09	762.6	$3/2^+$
		1177.9	0.27	1140.2	$5/2^+$
		1134.9	0.33	1183.1	$5/2^-$
		1009.3	0.18	1309.2	$3/2^+$
		964.0	0.16	1353.8	$3/2^-$
		939.5	0.35	1378.6	$5/2^+$
		709.7	0.22	1608.2	$(5/2^-)$
		539.0	0.12	1779.0	$5/2^-$
2327.3(2)					
		1564.7	0.16	762.6	$3/2^-$
2328.41(12)	$1/2^+, 3/2$				
		1855.2	0.15	473.2	$5/2^+$
		1705.0	0.11	623.0	$1/2^+$
		1545.7	0.33	782.6	$5/2^+$
		1188.4	0.16	1140.2	$5/2^+$
2338.04(14)	$(3/2^-)$				
		2338.6	0.24	0.0	$3/2^+$
		1865.0	0.20	473.2	$5/2^+$
		1835.6	0.08	501.9	$3/2^+$
		1706.4	0.08	631.4	$7/2^-$
		1555.4	0.09	782.6	$5/2^+$
		1154.5	0.19	1183.1	$5/2^-$
		729.9	0.03	1608.2	$(5/2^-)$
		558.7	0.08	1779.0	$5/2^-$
2339.64(13)	$1/2, 3/2$				
		2339.5	0.31	0.0	$3/2^+$
		2278.5	0.43	61.2	$1/2^+$
		1577.1	0.24	762.6	$3/2^+$
		1265.0	0.09	1075.0	$3/2^+$
2357.96(26)					
		1885.1	0.09	473.2	$5/2^+$
		1856.1	0.24	501.9	$3/2^+$
		1574.8	0.23	782.6	$5/2^+$
2359.82(26)	$3/2^-$				
		2359.4	0.24	0.0	$3/2^+$
		1578.3	0.12	782.6	$5/2^+$
		1175.7	0.10	1183.1	$5/2^-$
		751.5	0.12	1608.2	$(5/2^-)$
		580.6	0.11	1779.0	$5/2^-$
2391.42(24)	$(5/2^-)$				
		1760.2	0.10	631.4	$7/2^-$
		1605.6	0.08	786.1	$7/2^-$
		1208.2	0.05	1183.1	$5/2^-$
		612.1	0.06	1779.0	$5/2^-$
2429.1(2)	$3/2^+, 5/2^+$				
		2428.5	0.28	0.0	$3/2^+$
		1806.5	0.39	623.0	$1/2^+$
		1743.4	0.04	685.0	$7/2^+$
		1288.5	0.19	1140.2	$5/2^+$

Table 2 (*continued*)

E_i (keV)	Spin	E_γ (keV)	I_γ (%)	E_f (keV)	Spin
2438.37(9)	$(3/2^-)$				
		2438.4	0.06	0.0	$3/2^+$
		2377.3	0.26	61.2	$1/2^+$
		1936.7	0.21	501.9	$3/2^+$
		1675.8	0.13	762.6	$3/2^+$
		1655.5	0.22	782.6	$5/2^+$
2458.41(19)	$1/2^+$, 3/2, $5/2^+$				
		1984.8	0.13	473.2	$5/2^+$
		1836.1	0.05	623.0	$1/2^+$
		1676.0	0.22	782.6	$5/2^+$
		1149.1	0.06	1309.2	$3/2^+$
2468.92(3)	$1/2^-$				
		2469.0	2.36	0.0	$3/2^+$
		2407.9	0.83	61.2	$1/2^+$
		1967.0	0.97	501.9	$3/2^+$
		1845.9	0.18	623.0	$1/2^+$
		1706.5	2.17	762.6	$3/2^+$
		1394.1	0.05	1075.0	$3/2^+$
		1062.9	0.08	1405.9	$1/2^+$
		459.6	0.04	2009.8	$3/2^-$
2492.7(3)	3/2, $5/2^+$				
		1991.5	0.10	501.9	$3/2^+$
		1869.5	0.19	623.0	$1/2^+$
2496.82(13)	$(3/2^-)$				
		2435.5	0.91	61.2	$1/2^+$
		1313.2	0.23	1183.1	$5/2^-$
		889.1	0.08	1608.2	$(5/2^-)$
		717.9	0.20	1779.0	$5/2^-$
2519.5(3)	$5/2^-$, $7/2^-$				
		1888.3	0.09	631.4	$7/2^-$
		911.1	0.03	1608.2	$(5/2^-)$
2554.2(3)					
		2080.9	0.13	473.2	$5/2^+$
2561.26(13)	$(3/2^-)$				
		2561.8	0.23	0.0	$3/2^+$
		2500.2	0.11	61.2	$1/2^+$
		1378.0	0.14	1183.1	$5/2^-$
		1207.4	0.08	1353.8	$3/2^-$
		952.9	0.12	1608.2	$(5/2^-)$
		354.1	0.34	2206.8	$3/2^-$
		243.1	0.07	2317.9	$3/2^-$
2592.66(7)	$3/2^-$				
		2592.6	0.40	0.0	$3/2^+$
		2090.7	0.36	501.9	$3/2^+$
		1969.6	0.09	623.0	$1/2^+$
		1805.2	0.08	786.1	$7/2^-$
		1409.0	0.15	1183.1	$5/2^-$
		1283.5	0.06	1309.3	$3/2^+$
		1238.6	0.14	1353.8	$3/2^-$
		1187.2	0.13	1405.9	$1/2^+$

(*continued on next page*)

Table 2 (*continued*)

E_i (keV)	Spin	E_γ (keV)	I_γ (%)	E_f (keV)	Spin
		984.1	0.32	1608.2	$(5/2^-)$
		813.4	0.15	1779.0	$5/2^-$
		403.2	0.09	2189.5	$3/2^-, 5/2, 7/2^-$
2619.23(6)	$1/2^-$				
		2619.2	0.26	0.0	$3/2^+$
		2557.9	1.21	61.2	$1/2^+$
		2117.3	0.58	501.9	$3/2^+$
		1265.8	0.06	1353.8	$3/2^-$
		475.2	0.08	2144.1	$3/2^-$
2667.23(13)	$1/2^-$				
		2667.2	0.32	0.0	$3/2^+$
		2606.9	0.03	61.2	$1/2^+$
		2044.5	0.07	623.0	$1/2^+$
		1313.8	0.06	1353.8	$3/2^-$
2689.98(17)	$(3/2^-)$				
		2690.6	0.10	0.0	$3/2^+$
		2629.3	0.22	61.2	$1/2^+$
		2217.3	0.09	473.2	$5/2^+$
		2187.6	0.09	501.9	$3/2^+$
		2067.1	0.06	623.0	$1/2^+$
		2058.1	0.06	631.4	$7/2^-$
		1507.6	0.06	1183.1	$5/2^-$
2700.3(4)	1/2, 3/2				
		2700.5	0.45	0.0	$3/2^+$
2729.84(14)	$3/2^+$				
		2729.6	0.24	0.0	$3/2^+$
		2669.0	0.34	61.2	$1/2^+$
		1966.9	0.05	762.6	$3/2^+$
		1546.8	0.20	1183.1	$5/2^-$
2759.1(3)	$3/2^+$				
		2759.0	0.30	0.0	$3/2^+$
2762.5(4)	1/2, 3/2				
		2762.3	0.10	0.0	$3/2^+$
		2289.4	0.08	473.2	$5/2^+$
2773.09(12)	$3/2^-$				
		2773.7	0.07	0.0	$3/2^+$
		2711.8	0.10	61.2	$1/2^+$
		2299.4	0.09	473.2	$5/2^+$
		2271.0	0.14	501.9	$3/2^+$
		2150.3	0.08	623.0	$1/2^+$
		1987.3	0.08	786.1	$7/2^-$
		1698.7	0.03	1075.0	$3/2^+$
		1164.5	0.09	1608.2	$(5/2^-)$
		993.9	0.12	1779.0	$5/2^-$
		885.6	0.19	1888.6	$1/2^+$
2856.38(19)	$1/2^-$				
		2795.4	0.41	61.2	$1/2^+$
		1502.6	0.26	1353.8	$3/2^-$
2877.99(14)	3/2				
		2877.7	0.04	0.0	$3/2^+$

Table 2 (*continued*)

E_i (keV)	Spin	E_γ (keV)	I_γ (%)	E_f (keV)	Spin
		2816.8	0.20	61.2	$1/2^+$
		2404.9	0.07	473.2	$5/2^+$
		2376.4	0.11	501.9	$3/2^+$
		2115.8	0.08	762.6	$3/2^+$
		1693.9	0.06	1183.1	$5/2^-$
		1588.5	0.14	1289.7	$5/2^+$
2904.8(3)	1/2, 3/2				
		2430.1	0.08	473.2	$5/2^+$
		2404.0	0.13	501.9	$3/2^+$
		2122.1	0.38	782.6	$5/2^+$
2913.11(17)	$(1/2^-)$				
		2851.8	0.09	61.2	$1/2^+$
		2289.4	0.04	623.0	$1/2^+$
		2151.0	0.08	762.6	$3/2^+$
		1730.0	0.05	1183.1	$5/2^-$
		1559.9	0.07	1353.8	$3/2^-$
		1225.2	0.13	1687.6	$3/2^-$
2915.92(21)	3/2				
		2916.5	0.36	0.0	$3/2^+$
		2442.2	0.15	473.2	$5/2^+$
		2292.9	0.23	623.0	$1/2^+$
		1733.6	0.10	1183.1	$5/2^-$
		1561.6	0.10	1353.8	$3/2^-$
2932.00(22)	$3/2^-(1/2)$				
		2458.7	0.08	473.2	$5/2^+$
		2309.2	0.09	623.0	$1/2^+$
		1748.6	0.12	1183.1	$5/2^-$
		1623.8	0.08	1309.2	$3/2^+$
		1323.1	0.03	1608.2	$(5/2^-)$
2954.76(10)	$(3/2^-)$				
		2955.2	0.13	0.0	$3/2^+$
		2481.4	0.14	473.2	$5/2^+$
		2454.5	0.08	501.9	$3/2^+$
		2331.5	0.08	623.0	$1/2^+$
		2192.5	0.13	762.6	$3/2^+$
		1770.7	0.22	1183.1	$5/2^-$
		1346.6	0.07	1608.2	$(5/2^-)$
		1066.4	0.19	1888.6	$1/2^+$
		945.3	0.07	2009.8	$3/2^-$
2978.9(3)					
		2505.5	0.10	473.2	$5/2^+$
		1625.3	0.07	1353.8	$3/2^-$
2994.4(4)	$3/2^-$, 5/2, $7/2^-$				
		2492.1	0.15	501.9	$3/2^+$
		2363.3	0.10	631.4	$7/2^-$
3131.6(4)					
		2348.8	0.07	786.1	$7/2^-$
		1948.6	0.10	1183.1	$5/2^-$
3153.6(4)	$(3/2^-)$				
		3154.5	0.12	0.0	$3/2^+$

(*continued on next page*)

Table 2 (*continued*)

E_i (keV)	Spin	E_γ (keV)	I_γ (%)	E_f (keV)	Spin
		3093.9	0.08	61.2	$1/2^+$
		2680.1	0.07	473.2	$5/2^+$
		2371.4	0.10	782.6	$5/2^+$
		1306.2	–	1846.7	$3/2^+, 5/2^+$
3254.9(4)					
		2781.9	0.11	473.2	$5/2^+$
		2491.7	0.09	762.6	$3/2^+$
		2115.6	0.14	1140.2	$5/2^+$
3286.0(6)	1/2, 3/2				
		2664.6	0.08	623.0	$1/2^+$
		2523.4	0.05	762.6	$5/2^+$
3375.3(3)	$(3/2^-)$				
		2873.4	0.22	501.9	$3/2^+$
3391.77(16)	$3/2^-$				
		3392.2	0.05	0.0	$3/2^+$
		2918.6	0.17	473.2	$5/2^+$
		2769.6	0.11	623.0	$1/2^+$
		2630.7	0.05	762.6	$3/2^+$
		2209.0	0.11	1183.1	$5/2^-$
3416.02(22)	$3/2^-$				
		2943.6	0.11	473.2	$5/2^+$
		2912.8	0.16	501.9	$3/2^+$
		2793.4	0.16	623.0	$1/2^+$
		2653.2	0.16	762.6	$3/2^+$
		2233.4	0.17	1183.1	$5/2^-$
		1637.3	0.11	1779.0	$5/2^-$
3545.45(11)	$(3/2^-)$				
		3545.5	0.46	0.0	$3/2^+$
		3484.5	0.36	61.2	$1/2^+$
3567.36(23)	1/2, 3/2				
		3567.7	0.10	0.0	$3/2^+$
		3506.7	0.11	61.2	$1/2^+$
		3094.9	0.25	473.2	$5/2^+$
		3064.4	0.31	501.9	$3/2^+$
		2943.3	0.08	623.0	$1/2^+$
		2804.3	0.04	762.6	$3/2^+$
3572.2(6)	$(3/2^-)$				
		3099.0	0.07	473.2	$5/2^+$
3595.8(6)					
		3093.8	0.18	501.9	$3/2^+$
3679.36(25)	1/2, 3/2				
		3679.1	–	0.0	$3/2^+$
		3617.4	–	61.2	$1/2^+$
		2496.4	–	1183.1	$5/2^-$
		1649.4	–	2030.0	$(3/2^-), 5/2$
3719.6(4)	$1/2, 3/2, 5/2^+$				
		3719.0	0.05	0.0	$3/2^+$
		3659.0	0.06	61.2	$1/2^+$
		3218.5	0.06	501.9	$3/2^+$
		2956.1	0.06	762.6	$5/2^+$

Table 2 (*continued*)

E_i (keV)	Spin	E_γ (keV)	I_γ (%)	E_f (keV)	Spin
3764.49(15)	1/2, 3/2				
		3704.1	0.25	61.2	$1/2^+$
		2624.3	0.22	1140.2	$5/2^+$
		2580.8	0.08	1183.1	$5/2^-$
		2077.2	0.17	1687.6	$3/2^-$
3836.02(21)	1/2, 3/2				
		3836.0	0.23	0.0	$3/2^+$
		3776.3	0.11	61.2	$1/2^+$
		3334.6	0.13	501.9	$3/2^+$
3852.87(11)	3/2				
		3380.1	0.09	473.2	$5/2^+$
		3350.3	0.13	501.9	$3/2^+$
		2669.9	0.09	1183.1	$5/2^-$
3865.67(15)	$(3/2^-)$				
		3805.0	0.03	61.2	$1/2^+$
		3363.4	0.07	501.9	$3/2^+$
		3235.3	0.07	631.4	$7/2^-$
		2683.2	0.07	1183.1	$5/2^-$
		2061.0	0.04	1805.5	3/2
3883.52(17)	1/2, 3/2				
		3884.0	0.57	0.0	$3/2^+$
		3821.8	0.41	61.2	$1/2^+$
		3409.6	0.13	473.2	$5/2^+$
		2529.9	0.14	1353.8	$3/2^-$
3922.28(8)	1/2, 3/2				
		3922.7	0.06	0.0	$3/2^+$
		3861.0	0.27	61.2	$1/2^+$
		2568.7	0.15	1353.8	$3/2^-$
3954.1(5)	1/2, 3/2				
		3954.6	0.08	0.0	$3/2^+$
		3480.6	0.02	473.2	$5/2^+$
3973.70(20)	1/2, 3/2				
		3974.3	0.13	0.0	$3/2^+$
		3912.8	0.27	61.2	$1/2^+$
		2680.3	0.35	1293.2	$3/2, 5/2, 7/2^+$
4036.2(3)	1/2, 3/2				
		4036.3	–	0.0	$3/2^+$
		3975.4	–	61.2	$1/2^+$
4057.31(21)	1/2, 3/2				
		3996.5	0.12	61.2	$1/2^+$
		3584.0	0.08	473.2	$5/2^+$
6287.6(1)	$1/2^+$				
		6287.3	2.75	0.0	$3/2^+$
		6226.7	0.76	61.2	$1/2^+$
		5814.1	0.48	473.2	$5/2^+$
		5785.5	0.87	501.9	$3/2^+$
		5664.1	0.98	623.0	$1/2^+$
		5212.4	0.19	1075.0	$3/2^+$
		4977.8	0.22	1309.2	$3/2^+$
		4934.0	1.84	1353.8	$3/2^-$

(*continued on next page*)

Table 2 (*continued*)

E_i (keV)	Spin	E_γ (keV)	I_γ (%)	E_f (keV)	Spin
		4600.8	–	1687.6	$3/2^-$
		4514.2	0.85	1773.0	$3/2^+$
		4482.3	0.23	1805.5	$1/2^+$, 3/2
		4420.0	0.29	1867.8	3/2
		4410.3	–	1877.9	$1/2^+$, 3/2, $5/2^+$
		4399.1	0.39	1888.6	$1/2^+$
		4331.2	0.44	1956.3	$3/2^+$
		4295.0	0.45	1992.7	3/2, $(1/2^+)$
		4277.8	2.15	2009.8	$3/2^-$
		4179.0	0.31	2109.1	$1/2^+$, 3/2, $5/2^+$
		4167.3	0.21	2120.0	$1/2^+$
		4149.7	0.25	2138.2	$1/2^+$, 3/2, $5/2^+$
		4143.5	2.34	2144.1	$3/2^-$
		4131.1	–	2156.8	1/2, 3/2, $5/2^+$
		4112.3	0.27	2175.7	$(3/2^+)$
		4080.8	13.00	2206.8	$3/2^-$
		4041.7	0.55	2246.1	$3/2^-$
		3969.6	2.39	2317.9	$3/2^-$
		3959.1	0.33	2328.4	$1/2^+$, 3/2
		3949.6	0.31	2338.0	$(3/2^-)$
		3928.8	0.23	2359.5	$3/2^-$
		3858.0	0.43	2429.1	$3/2^+$, $5/2^+$
		3849.2	0.53	2438.4	$(3/2^-)$
		3818.7	6.37	2468.9	$1/2^-$
		3790.7	0.63	2496.8	$(3/2^-)$
		3726.3	0.42	2561.3	$(3/2^-)$
		3694.8	1.43	2592.7	$3/2^-$
		3668.2	1.47	2619.2	$1/2^-$
		3620.6	0.60	2667.2	$1/2^-$
		3597.7	0.21	2690.0	$(3/2^-)$
		3586.3	0.18	2700.3	1/2, 3/2
		3557.7	0.59	2729.9	$3/2^+$
		3528.4	0.42	2759.1	$3/2^+$
		3524.2	0.16	2762.5	1/2, 3/2
		3514.6	0.57	2773.1	$3/2^-$
		3431.5	0.19	2856.4	$1/2^-$
		3409.7	0.41	2878.0	3/2
		3382.4	0.48	2904.8	1/2, 3/2
		3374.3	0.43	2913.1	$(1/2^-)$
		3372.1	0.92	2915.9	3/2
		3355.9	0.26	2932.0	$3/2^-$, (1/2)
		3332.9	0.86	2954.8	$3/2^-$
		2896.0	0.54	3391.8	$3/2^-$
		2871.5	0.35	3416.0	$3/2^-$
		2742.2	0.68	3545.4	$(3/2^-)$
		2720.6	0.33	3567.4	1/2, 3/2
		2608.7	0.59	3679.4	1/2, 3/2
		2523.1	0.82	3764.5	1/2, 3/2
		2451.5	0.32	3836.0	1/2, 3/2
		2434.8	0.66	3852.9	$3/2^-$
		2422.1	0.52	3865.7	$(3/2^-)$

Table 2 (*continued*)

E_i (keV)	Spin	E_γ (keV)	I_γ (%)	E_f (keV)	Spin
		2404.0	0.48	3883.5	1/2, 3/2
		2365.3	0.95	3922.3	1/2, 3/2
		2314.0	0.39	3973.7	1/2, 3/2
		2250.9	0.22	4036.2	1/2, 3/2
		2230.4	0.40	4057.3	1/2, 3/2

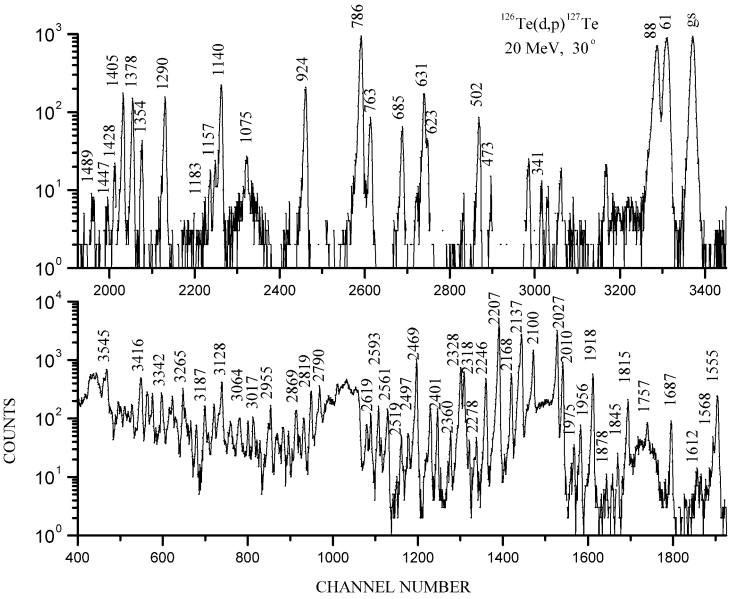

Fig. 2. Example of the spectrum from the ^{126}Te$(d, p)^{127}$Te reaction measured at a scattering angle of 30° with the polarized deuteron beam in the magnetic substate $m = -1$. The peaks labeled with the level energy in keV belong to ^{127}Te.

appear at higher energies where due to the high level density it is often hard to relate the levels seen in both reactions. To avoid errors of incorrect level identification with unclear angular and asymmetry dependence in this region the calibration curve of the higher part of spectra was iteratively improved as more levels were analyzed also by inclusion of multi-step processes. We found that the old Q-value of 4.044(8) MeV reported by Graue et al. [17] differs from our value of 4.063(1) MeV obtained from the neutron binding energy of neutron capture in ^{126}Te. For this reason all the excitation energies listed in Ref. [17] are gradually shifted to the lower side. The maximum deviation in energy reaches 19 keV at 2 MeV. Weighted mean energies from all angles and absolute intensities of the (d, p) peaks are listed in Table 4.

2.3. DWBA and CC analysis

The angular distributions of cross section and asymmetry in (d, p) with polarized deuterons show pronounced oscillations. From their very distinct patterns the determi-

Table 3
Optical-model parameters used in DWBA and CC calculations

	V (MeV)	r_v (fm)	a_v (fm)	$4W'_D$ (MeV)	r_w (fm)	a_w (fm)	V_{ls} (MeV)	r_{ls} (fm)	a_{ls} (fm)	r_c (fm)	nlc[a]
d	80.39	1.16	0.84	84.9	1.35	0.73	15.6[b]	1.16	0.84	1.20	0.54
p	52.65	1.22	0.67	44.0	1.23	0.67	30.0[c]	1.22	0.67	1.25	0.85
n	[d]	1.26	0.69				+25.0				0.85

[a] Nonlocal range parameter.
[b] Multiplied by 2 in accordance with CHUCK3.
[c] Multiplied by 4 in accordance with CHUCK3.
[d] Well depth adjusted to reproduce the binding energy.

nation of the transferred orbital l and total angular momentum j (with $j = l + 1/2$ and $j = l - 1/2$) becomes obvious by comparison to distorted-wave Born-approximation (DWBA) calculations. The differential cross sections and vector-analyzing powers were calculated using the code CHUCK3 [33]. The parameters for the optical potentials of the deuteron and proton waves given in Table 3 were chosen close to the 'global' sets [34,35] and have been kept practically constant for all Te isotopes investigated by us (see also ^{131}Te [13]). The recommended finite range correction 0.621 and the non-locality parameter 'nlc' listed in Table 3 were taken into account. The (d, p) spectroscopic strengths were obtained by a fit of the experimental data using the relation

$$\left(\frac{d\sigma}{d\Omega}\right)_{\text{exp}} = S_{lj}\sigma_{lj}, \tag{1}$$

where S_{lj} is the spectroscopic factor and σ_{lj} the calculated (DWBA) differential cross section. The calculated DWBA asymmetries were also compared with the experimental ones which were deduced from the equation

$$A_y(\text{exp}) = \frac{2}{3P_y} \cdot \frac{\sigma_+ - \sigma_-}{\sigma_+ + \sigma_-}, \tag{2}$$

where σ_+ and σ_- are the experimental cross sections at each angle for spin up and spin down with a vector polarization P_y, respectively.

Experimental angular distributions for most of the levels are well reproduced by the calculations indicating direct, one-step stripping mechanisms. The strengths S_{lj} extracted in the present work and listed in Table 4 are in good overall agreement, at least for the strong peaks, with the previous studies [17,18] taking into account a systematic shift of their excitation energies. Comparing both the experimental asymmetries and the calculated ones we found that the experimental curves often are shifted to the positive or negative side with respect to the zero line. This could be partly due to the background conditions in each case. Some levels at low energies deserve special attention since here we have practically no background. The distinct type of asymmetry was observed for the both $1/2^+$ states at 61 and 623 keV. The characteristic oscillations of the angular distributions of asymmetry are also often shifted to other angles with respect to the DWBA curves. In these cases it seems that the angular dependence of A_y is more sensitive to the reaction mechanism than to the optical potential. In general, the agreement between the calculated shapes and the

Table 4
Summary of the ^{127}Te levels observed in the (n,γ), (d,p) reactions and other studies, including energies, spin-parities and spectroscopic strengths

(n,γ)	(d,p)[a]					Pick-up studies [19]				Adopted	
Level energy (keV)	Level energy (keV)	$\frac{d\sigma}{d\Omega}$ (20°) ($\frac{\mu b}{sr}$)	l	J^π	$S_{lj}\times 100$	Level energy (keV)	l	J^π	$(2J+1)S_{lj}$	Level energy (keV)	J^π
0.0	0.0(2)	1581	2	$3/2^+$	24	0	2	$3/2^+$	2.5	0	$3/2^+$
61.17(1)	61.1(2)	739[c]	0	$1/2^+$	20	62	0	$1/2^+$	1.5	61.17(1)	$1/2^+$
88.20(5)	88.3(2)	582[c]	5	$11/2^-$	23	89	5	$11/2^-$	5.5	88.20(5)	$11/2^-$
340.88(5)	341.2(4)	4[c]	(5)	$(9/2^-)$	0.4[h]	340	(5)	$9/2^-$	(0.02)	340.88(5)	$9/2^-$
473.21(3)	472.7(3)	10	2	$5/2^+$	0.02[h]	475	2	$5/2^+$	0.008	473.21(3)	$5/2^+$
501.93(1)	501.2(2)	142	2	$3/2^+$	1.3	503	2	$3/2^+$	0.07	501.93(1)	$3/2^+$
						603	2	$(5/2^+)$	0.03		
622.98(2)	624.6(3)	24[c]	0	$1/2^+$	0.7					622.98(2)	$1/2^+$
631.41(5)	632.4(2)	114	3	$7/2^-$	0.8[h]	633	3	$7/2^-$	0.11	631.41(5)	$7/2^-$
684.99(5)	685.5(3)	26[c]	4	$7/2^+$	0.2[h]	687	4	$7/2^+$	0.56	685.00(6)	$7/2^+$
762.57(3)	763.0(2)	126	2	$3/2^+$	0.4	763				762.57(3)	$3/2^+$
782.63(3)						783	2	$5/2^+$	1.7	782.63(3)	$5/2^+$
786.12(5)	786.0(2)	768	3	$7/2^-$	4.9					786.12(5)	$7/2^-$
923.90(16)	924.3(3)	77[c]	4	$7/2^+$	3.0	926	4	$7/2^+$	3.9	923.90(16)	$7/2^+$
						966	2	$(5/2^+)$	0.01		
1074.98(5)	1074.8(2)	27	2	$3/2^+$	0.1[h]	1075	2	$5/2^+$	0.03	1074.98(5)	$3/2^+$
1077.11(22)										1077.11(22)	[b] $5/2^+, 9/2^+$
1140.23(4)	1140.6(2)	155	2	$5/2^+$	1.1	1140	2	$5/2^+$	0.87	1140.23(4)	$5/2^+$
1154.67(9)										1154.67(9)	$5/2, 7/2^+$
	1156.8(3)	8[c]		$(11/2^-)$	0.06[h]	1157	(5)	$11/2^-$	0.18	1156.8(3)	$11/2^-$
1183.12(5)	1183.0(3)	4								1183.12(5)	$5/2^-$
						1206	2	$(5/2^+)$	0.009	1206?	$(5/2^+)$
1289.72(8)	1290.6(2)	94	2	$5/2^+$	0.7[h]	1290	2	$5/2^+$	0.53	1289.72(8)	$5/2^+$
1293.15(8)										1293.15(8)	$3/2^+, 5/2, 7/2^+$
1309.27(8)	1308.3(5)	4				1308	2	$(5/2^+)$	0.02	1309.27(8)	$3/2^+$
1353.78(6)	1353.1(2)	11	1	$3/2^-$	0.12[h]	1354	(1)	$(3/2^-$	0.005	1353.78(6)	$3/2^-$
1378.59(8)	1378.9(2)	91	2	$5/2^+$	0.62[h]	1378	2	$5/2^+$	0.61	1378.59(8)	$5/2^+$
1405.88(20)	1405.1(2)	63[c]	0	$1/2^+$	1.4	1405	0	$1/2^+$	0.05	1405.88(20)	$1/2^+$

(*continued on next page*)

Table 4 (*continued*)

(n,γ)	(d,p)[a]					Pick-up studies [19]				Adopted	
Level energy (keV)	Level energy (keV)	$\frac{d\sigma}{d\Omega}$ (20°) ($\frac{\mu b}{sr}$)	l	J^π	$S_{lj}\times 100$	Level energy (keV)	l	J^π	$(2J+1)S_{lj}$	Level energy (keV)	J^π
1429.0(3)	1428.1(2)	5[c]	4	$7/2^+$	[h]	1429	4	$7/2^+$	0.16	1429.0(3)	$7/2^+$
	1447.4(3)	3[c]				1447	(4)	$(7/2^+)$	0.12	1447.4(3)	$(7/2^+)$
1462.14(22)										1462.14(22)	$3/2^+, 5/2, 7/2^+$
1491.7(3)	1489.4(8)[d]	4[c]				1491	(4)	$(7/2^+)$	0.14	1491.7(3)	$(7/2^+)$
1550.64(10)	1549.7(3)	8								1550.64(10)	$(7/2^-, 5/2^-)$
1555.7(6)	1555.2(2)	161	2	$5/2^+$	1.2	1554	2	$5/2^+$	1.1	1555.7(6)	$5/2^+$
1568.05(10)	1567.6(2)	23	2	$5/2^+$	0.16	1567	2	$(5/2^+)$	0.11	1568.05(10)	$5/2^+$
	1602.3(6)	3[c]				1602	(2)	$(5/2^+)$	0.01	1602.3(6)	$(5/2^+)$
1608.19(6)										1608.19(6)	$(5/2^-)$
1612.1(5)	1612.8(4)	5[c]	4		[h]	1614	4	$(7/2^+)$	0.35	1612.1(5)	$(7/2^+)$
1683.4(4)[i]						1683	2	$(5/2^+)$	0.01	1683.4(4)	$(5/2^+)$
1687.59(11)	1687.4(2)	20	1	$3/2^-$	0.32					1687.59(11)	$3/2^-$
1704.22(18)						1702	2	$(5/2^+)$	0.01	1704.22(18)	$3/2^+, 5/2^+$
	1731.8(13)	2[c]				1732	(4)	$(7/2^+)$	0.11		
1758.4(3)	1757.1(2)	27	(2), 3	$7/2^-$	0.06[h]					1758.4(3)	$7/2^-$
1773.02(4)	1774.0(8)	5				1770	2	$(5/2^+)$	0.02	1773.02(4)	$3/2^+$
1778.99(8)	1779.9(5)	4								1778.99(8)	$5/2^-$
1803.41(20)[i]	1804.5(8)	2[c]				1804	4	$7/2^+$	0.21	1803.41(20)	$7/2^+$
1805.51(8)										1805.51(8)	$1/2^+, 3/2$
1815.3(4)	1814.8(2)	76	(2), 3	$7/2^-$	0.49					1815.3(4)	$7/2^-$
1844.82(20)	1844.0(3)	12	3	$5/2^-$	0.1					1844.82(20)	$5/2^-$
1846.7(8)										1846.7(8)	$3/2^+, 5/2^+$
1868.2(2)										1868.2(2)	$1/2^+, 3/2, 5/2^+$
1877.88(14)	1878.4(4)	9				1875	2	$(5/2^+)$	0.11	1877.88(14)	$1/2^+, 3/2, 5/2^+$
1883.79(19)										1883.79(18)	$(5/2^-)$
1888.61(12)						1887	0	$1/2^+$	0.03	1888.61(12)	$1/2^+$
1916.0(4)[i]						1914	2	$(3/2^+)$	0.02	1916.0(4)	$(3/2^+)$
1919.3(3)	1918.2(2)	226	(2), 3	$7/2^-$	1.4					1919.3(3)	$7/2^-$
	(1943)					1938	4	$7/2^+$	0.37	1938	$7/2^+$

Table 4 (*continued*)

(n,γ)	(d,p)[a]					Pick-up studies [19]				Adopted	
Level energy (keV)	Level energy (keV)	$\frac{d\sigma}{d\Omega}$ (20°) ($\frac{\mu b}{sr}$)	l	J^π	$S_{lj}\times 100$	Level energy (keV)	l	J^π	$(2J+1)S_{lj}$	Level energy (keV)	J^π
1956.26(6)	1956.4(2)	20	(1, 2)	$(3/2^-)$	0.2	1954	0	$1/2^+$	0.07	1956.26(6)	$3/2^+$
1959.22(18)	(1960.7(6))									1959.22(18)	$(3/2^-)$
1975.5(3)	1975.5(2)	10	(2), 3	$(5/2^+)$, $7/2^-$		1974	2	$(5/2^+)$	0.04	1975.5(3)	$(5/2^+)$, $7/2^-$
	1985.2(3)	3[c]	(4)	$(7/2^+)$		1985	(4)	$(7/2^+)$	0.29	1985.2(3)	$(7/2^+)$
1992.68(14)										1992.68(14)	$3/2$ $(1/2^+)$
	(2001.7(4))	4				1998	1	$(3/2^-)$	0.02	2001.7(4)	$(3/2^-)$
2009.83(5)	2009.7(1)	193	1	$3/2^-$	2.7	2008	(0)	$(1/2^+)$	0.02	2009.83(5)	$3/2^-$
2025.9(5)	2026.7(1)	1258	3	$7/2^-$	7.1	2026	2	$(5/2^+)$	0.03	2025.9(5)	$7/2^-$
2030.00(10)										2030.00(10)	$3/2^-, 5/2, 7/2^+$
2048.61(14)	(2047.9(5))	12				2051	(2)	$(5/2^+)$	0.02	2048.61(14)	$1/2^+, 3/2, 5/2^+$
2056.27(11)										2056.27(11)	$3/2^+, 5/2, 7/2^+$
	2099.8(1)	555	3	$7/2^-$	3.2	2098	2	$(5/2^+)$	0.02	2099.8(1)	$7/2^-$
2101.8(3)[i]										2101.8(3)	
2109.12(12)										2109.12(12)	$1/2^+, 3/2, 5/2^+$
2119.96(15)	2120.0(7)	14				2117	0	$1/2^+$	0.1	2119.96(15)	$1/2^+$
	2137.5(2)	1344	3	$7/2^-$	7.5	2137	(4)	$(7/2^+)$	0.34	2137.5(2)	$7/2^-$
2138.11(22)										2138.11(22)	$1/2^+, 3/2$
2144.15(5)	2145.1(3)	136	1	$3/2^-$	1.8					2144.15(5)	$3/2^-$
2156.8(2)[i]										2156.8(2)	$1/2, 3/2, 5/2^+$
2167.1(3)[i]	2168.2(2)	229	3	$7/2^-$	1.3					2168.2(2)	$7/2^-$
2175.67(21)						2174	2	$(5/2^+)$	0.03	2175.67(21)	$(3/2^+)$
2189.53(23)	2190.2(3)	4								2189.53(23)	$3/2^-, 5/2, 7/2^-)$
						2196	4	$7/2^+$	0.44		
2206.76(1)	2206.7(1)	1046	1	$3/2^-$	14					2206.76(1)	$3/2^-$
2224.88(14)	2223.7(8)	10				2217	2	$(5/2^+)$	0.03	2224.88(14)	$1/2^+, 3/2, 5/2^+$
2243.6(4)						2242	(4)	$(7/2^+)$	0.17	2243.6(4)	$(7/2^+)$
2246.07(13)	2247.3(1)	117	1	$3/2^-$	1.7					2246.07(13)	$3/2^-$
2254.12(20)										2254.12(20)	5/2, (7/2)
2278.32(25)	2278.4(2)	22	3	$5/2^-$	0.19	2279	(2)	$(5/2^+)$	0.02	2278.32(25)	$(5/2^-)$

(*continued on next page*)

Table 4 (*continued*)

(n,γ)	(d,p)[a]					Pick-up studies [19]				Adopted	
Level energy (keV)	Level energy (keV)	$\frac{d\sigma}{d\Omega}$ (20°) ($\frac{\mu b}{sr}$)	l	J^π	$S_{lj}\times 100$	Level energy (keV)	l	J^π	$(2J+1)S_{lj}$	Level energy (keV)	J^π
2300.1(5)	2300.3(3)	20	(2), 3	$5/2^-$	0.15					2300.1(5)	$5/2^-$
2304.7(3)[i]										2304.7(3)	
2317.90(5)	2317.2(1)	144	1	$3/2^-$	1.9					2317.90(5)	$3/2^-$
2327.3(2)[i]										2327.3(2)[i]	
	2327.7(2)	334	3	$7/2^-$	1.7					2327.7(2)	$7/2^-$
2328.41(12)										2328.41(12)	$1/2^+, 3/2$
2338.04(14)	2340.2(7)	12	(1)	$(3/2^-)$	(0.15)					2338.04(14)	$(3/2^-)$
2339.64(13)										2339.64(13)	$1/2, 3/2$
2357.96(26)										2357.96(26)	
2359.82(26)	2360.5(3)	12	1	$3/2^-$	0.15					2359.82(26)	$3/2^-$
	2368.3(4)	4								2368.3(4)	$7/2^+$
2391.42(24)	2392.4(9)	5								2391.42(24)	$(5/2^-)$
	2401.3(2)	56	3	$7/2^-$	0.17					2401.3(2)	$7/2^-$
	2427.0(4)[e]	35								2427.0(4)	
2429.1(2)										2429.1(2)	$3/2^+, 5/2^+$
2438.37(9)	2438.2(5)	7	(1)	$(3/2^-)$						2438.37(9)	$(3/2^-)$
2458.41(19)						2461	(0)	$(1/2^+)$	0.01	2458.41(19)	$1/2^+, 3/2, 5/2^+$
2468.92(3)	2469.3(2)	299	1	$1/2^-$	8.1					2468.92(3)	$1/2^-$
						2473	(2)	$(5/2^+)$	0.06		
2492.7(3)										2492.7(3)	$3/2, 5/2^+$
2496.82(13)	2494.7(3)	88	2(3)	$3/2^+, (5/2^-)$						2496.82(13)	$(3/2^-)$
2519.5(3)	2518.9(2)	21	(2, 3)							2519.5(3)	$5/2^-, 7/2^-$
2554.2(3)[i]										(2554.2(3))	
2561.26(13)	2562.9(5)[g]	69	(1), 2	$3/2^-, 5/2^+$	(0.3, 0.46)					2561.26(13)	$(3/2^-)$
2592.66(7)	2592.7(3)	125	(1, 3)	$(3/2^-, 7/2^-)$	(0.3)					2592.66(7)	$3/2^-$
2619.23(6)	2618.9(3)	31	1	$1/2^-$	0.91					2619.23(6)	$1/2^-$
2667.23(13)	2667.6(4)	22	1	$1/2^-$	0.68					2667.15(13)	$1/2^-$
2689.98(17)	2691.8(7)	12								2689.98(17)	$(3/2^-)$

Table 4 (*continued*)

(n,γ)	(d,p)[a]					Pick-up studies [19]				Adopted	
Level energy (keV)	Level energy (keV)	$\frac{d\sigma}{d\Omega}$ (20°) ($\frac{\mu b}{sr}$)	l	J^π	$S_{lj}\times 100$	Level energy (keV)	l	J^π	$(2J+1)S_{lj}$	Level energy (keV)	J^π
2700.3(4)	2699.3(4)[g]	27								2700.3(4)	1/2, 3/2
	2713.2(2)	22								2713.2(2)	
2729.84(14)	2730.6(3)	119	2	$3/2^+$	0.4					2729.84(14)	$3/2^+$
2759.1(3)	2759.3(2)	48	2	$3/2^+$	0.1					2759.1(3)	$3/2^+$
2762.5(4)[i]										(2762.5(4))	1/2, 3/2
	2767.2(2)	42	2, (3)	$3/2^+$, $(5/2^-)$	0.1					2767.2(2)	$3/2^+$, $(5/2^-)$
2773.09(12)										2773.09(12)	$(3/2^-)$
	2782.9(3)	15	(3)	$(7/2^-)$	(0.04)					2782.9(3)	$(7/2^-)$
	2789.8(3)	193	3	$5/2^-$	1.4					2789.8(3)	$5/2^-$
	2799.1(4)	21								2799.1(4)	
	2818.9(2)	203	3	$5/2^-$	1.6					2818.9(2)	$5/2^-$
	2843.7(3)[g]	52	(1)	$(1/2^-)$						2843.7(3)	$(1/2^-)$
2856.38(19)	2858.6(3)	13	1	$1/2^-$	0.3					2856.38(19)	$1/2^-$
	2869.3(6)[g]	74	(3)	$(5/2^-)$						2869.3(6)	$(5/2^-)$
2877.99(14)										2877.99(14)	3/2
	2895.6(5)	19	2, 3	$5/2^+$, $7/2^-$	(0.14, 0.1)					2895.6(5)	$5/2^+$, $7/2^-$
2904.8(3)										2904.8(3)	1/2, 3/2
2913.11(17)	2913.9(4)	23	(1)	$(1/2^-)$						2913.11(17)	$(1/2^-)$
2915.92(21)										2915.92(21)	3/2
	2925.3(4)	10	(1)	$(3/2^-)$	0.07[h]					2925.3(4)	$(3/2^-)$
2932.00(22)	2934.6(7)[f]	25								2932.00(22)	$(1/2), 3/2^-$
2954.76(10)	2957.0(5)	50	(1)	$(3/2^-)$	0.4[h]					2954.76(10)	$(3/2^-)$
	2966.1(5)	34	(2, 3)							2966.1(5)	
2978.9(3)[i]										(2978.9(3))	
2994.4(4)	2994.4(6)	31								2994.4(4)	$3/2^-, 5/2, 7/2^+$
	3004.8(8)	40								3004.8(8)	
	3017.2(5)	47	2, 3	$(5/2^+), 7/2^-$	0.23					3017.2(5)	$7/2^-(5/2^+)$
	3035.4(4)	19	2, 3	$(5/2^+), 7/2^-$	0.15					3035.4(4)	$7/2^-(5/2^+)$

(*continued on next page*)

Table 4 (*continued*)

(n,γ)	(d,p)[a]					Pick-up studies [19]				Adopted	
Level energy (keV)	Level energy (keV)	$\frac{d\sigma}{d\Omega}$ (20°) ($\frac{\mu b}{sr}$)	l	J^π	$S_{lj}\times 100$	Level energy (keV)	l	J^π	$(2J+1)S_{lj}$	Level energy (keV)	J^π
	3064.0(7)[g]	23	(1)	$(3/2^-)$						3064.0(7)	$(3/2^+)$
	3096.1(6)[g]	24	2, 3	$(5/2^+)$, $7/2^-$	0.12					3096.1(6)	$7/2^-(5/2^+)$
	3127.6(4)	140	3	$7/2^-$	0.7					3127.6(4)	$7/2^-$
3131.6(4)[i]										(3131.6(4))	
	3138.1(7)	28								3138.1(7)	
3153.7(6)	3154.8(4)	60	(1), 3	$(3/2^-)$, $7/2^-$	0.3					3153.7(6)	$(3/2^-)$
	3175.5(5)	15								3175.5(5)	
	3187.4(4)	53	(3)	$(7/2^-)$	(0.27)					3187.4(4)	$7/2^-$
	3218.1(5)	22								3218.1(5)	
	3237.6(6)	32	(2, 3)							3237.6(6)	
	3251.9(5)	20								3251.9(5)	
3254.9(4)										3254.9(4)	
	3265.3(6)	95	(2, 3)							3265.3(6)	
3286.0(6)[i]	3286.5(7)	26								3286.0(6)	
	3303.9(6)	65								3303.9(6)	
	3314.4(5)	21								3314.4(5)	
	3341.7(4)	69	2, 3							3341.7(4)	
3375.3(3)[i]	3375.9(8)	91	(1, 3)	$(3/2^-, 7/2^-)$	(0.8, 0.4)					3375.3(3)	$(3/2^-)$
3391.77(16)	3394.6(8)	91	1	$3/2^-$	0.9					3391.77(16)	$3/2^-$
3416.02(22)	3416.6(4)	122	1	$3/2^-$	1.9					3416.21(27)	$3/2^-$
	3450.3(6)	29	1	$3/2^-$	0.4					3450.3(6)	
	3479.8(10)	24								3479.8(10)	
	3502.5(7)[g]	24								3502.5(7)	
3545.45(11)	3544.9(5)	90	(1)	$(3/2^-)$	2.4					3545.45(11)	$(3/2^-)$
	3553.8(5)	33								3553.8(5)	
3567.36(23)										3567.25(21)	1/2, 3/2
3572.2(6)[i]	3572.0(6)	25	(1)	$(3/2^-)$	(0.7)					3572.2(6)	$(3/2^-)$
	3582.9(5)	49								3582.9(5)	

Table 4 (*continued*)

(n,γ)	(d,p)[a]					Pick-up studies [19]				Adopted	
Level energy (keV)	Level energy (keV)	$\frac{d\sigma}{d\Omega}$ (20°) ($\frac{\mu b}{sr}$)	l	J^π	$S_{lj}\times 100$	Level energy (keV)	l	J^π	$(2J+1)S_{lj}$	Level energy (keV)	J^π
3595.8(6)	3595.5(5)	32								3595.8(6)	
	3608.9(7)	18								3608.9(7)	
	3652.8(9)	9								3652.8(9)	
3679.36(25)										3679.36(25)	1/2, 3/2
3719.6(4)										3719.6(4)	$1/2, 3/2, 5/2^+$
3764.49(15)										3764.49(15)	1/2, 3/2
3836.02(21)										3836.02(21)	1/2, 3/2
3852.87(11)										3852.87(11)	3/2
3865.67(15)										3865.67(15)	1/2, 3/2
3883.52(17)										3883.52(17)	1/2, 3/2
3922.28(8)										3922.28(8)	1/2, 3/2
3954.1(5)[i]										3954.1(5)	1/2, 3/2
3973.70(20)										3973.70(20)	1/2, 3/2
4036.2(3)										4036.2(3)	1/2, 3/2
4057.31(21)										4057.31(21)	1/2, 3/2

[a] Weighted average value over the all angle measurements. [b] Spin and parity assignment from β decay [29]. [c] Cross section at $\Theta = 30°$. [d] May belong to ^{129}Te. [e] Contaminated by ^{129}Te. [f] Contaminated by ^{131}Te. [g] Could be a doublet. [h] Pure CCBA. The upper limit of the direct contribution is given. [i] Tentative level.

experimental data points is satisfactory up to 2.6 MeV where most of the (d, p) peaks are rather well resolved. Thus in most cases excluding some of the weakest (d, p) peaks the l-values are clearly identified. Typical examples of the calculated angular distributions of cross section and asymmetry and measured data points are shown in Figs. 3 and 4.

Inclusion of multi-step processes in the DWBA analysis significantly improves in many cases the agreement with the experimental data. The multi-step or the inelastic-transfer processes take place in both the ^{126}Te target channel (through the 2^+, 4^+, etc. excitations) and in the final ^{127}Te nucleus through the excitation of members of the multiplet coupled by collective matrix elements. The coupled channels (CC) were selected with the collective and single-particle form factors according to prescriptions of Ref. [33]. In the calculations we used the deformation parameter $\beta_2 = 0.153$ [36] derived from the $B(\mathrm{E2})\uparrow$ value for the first 2^+ in the ^{126}Te. The same value of the β_2 was used for the ^{127}Te final nucleus. Since the transfer step $2^+ \to J$ is usually not well known we assumed this transfer to be of the lowest multipolarity. The subsequent spectroscopic amplitudes were freely varied in accordance with the χ^2 value of the fit to the experimental cross sections and asymmetry data. From the fitting procedure we found that a least squares fit of the angular distribution data does not often give a suitable asymmetry shape. In these cases we gave a preference to the asymmetry fit. The experimental data were analyzed by supposing that all coupled channels yield a coherent sum so that the percentage of each step could be determined from the shape fit of the experimental angular distributions and asymmetries. With respect to the direct one-step transfer the two-step angular distributions alone are rather washed out and they do not so much disturb the final angular picture. To the contrary, the asymmetry distributions are particularly sensitive to inelastic transfer admixtures which can significantly change not only the shape but even the sign of the A_y distribution. We found that the experimental asymmetries of even the lowest 'hole' states including the ground state are influenced by multi-step processes indicating their more complicated structures. We also notice that the application of the one-step DWBA route alone leads for most $3/2^-$ states to a wrong curvature of the angular distributions after the second maximum. Since the complexity of the wave function grows rapidly with excitation energy the choice of proper 'coupled-channels' and corresponding phases of their amplitudes becomes non-trivial. Thus only for the lowest states it is possible to find the right inelastic route. The extracted spectroscopic factors S_{lj} given in Table 4 correspond to the contribution of the direct one-step transfer. In general they are somewhat smaller than the earlier reported values [17,18] which were obtained neglecting multi-step contributions.

3. Level scheme

3.1. Level energies and quantum number assignments

The previous level scheme of ^{127}Te [16] was greatly extended using the present experimental data from the (n, γ) coincidence measurements and the (d, p) reaction with polarized deuterons. Numerous γ-transitions observed in the present work were placed in the level scheme due to the coincidence relationships. Intensities of unresolved multiplets in the single spectrum were determined using the coincidence information of separate

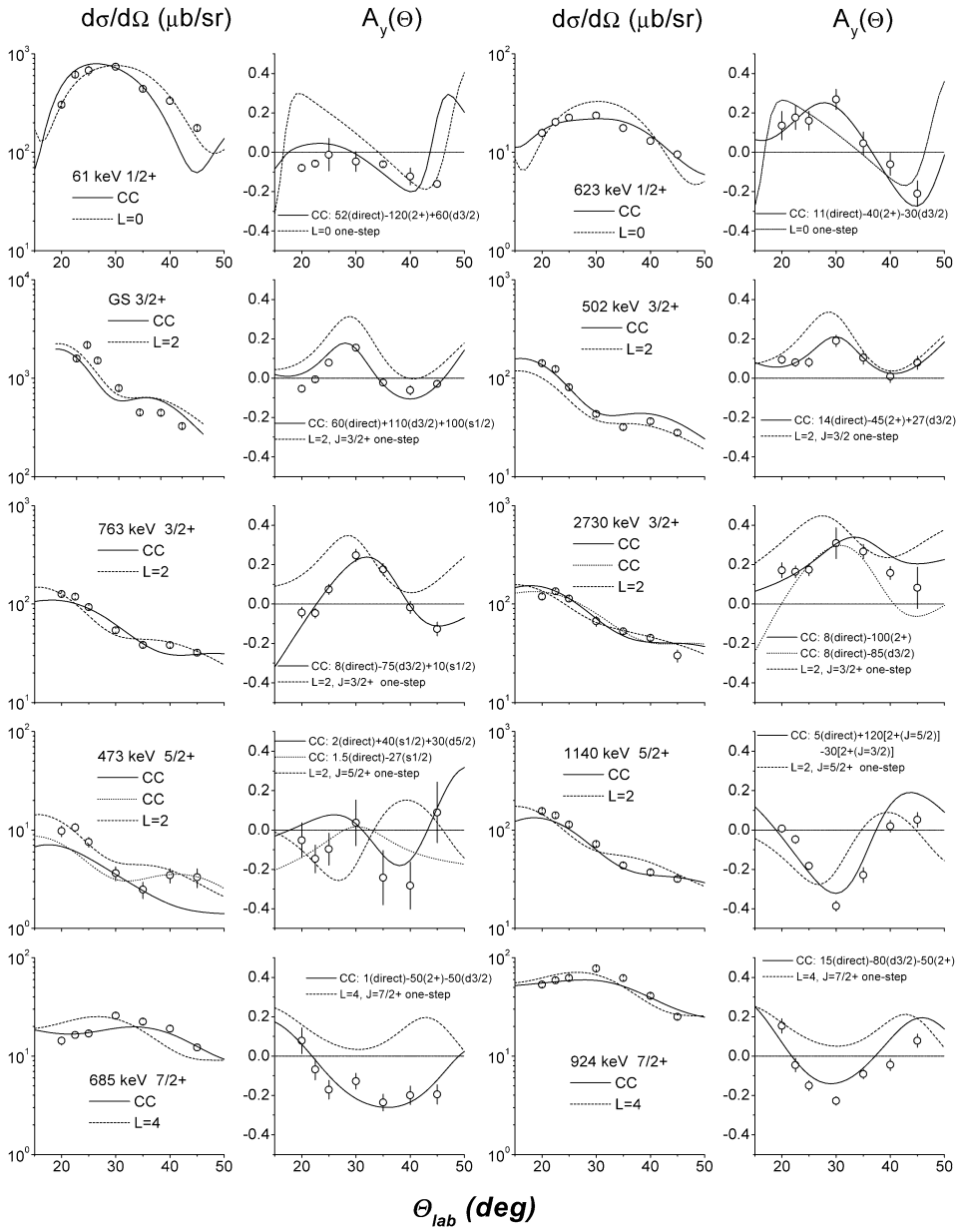

Fig. 3. Angular distributions of the differential cross sections and of the asymmetries for the ^{126}Te($\vec{d}$, p)^{127}Te reaction measured at 20 MeV for levels with positive parity. The circles are experimental values. The dashed lines represent DWBA calculations for pure direct one-step transfers. The solid lines result from the CCBA calculations and various contributions are shown in the figures with phases and corresponding amplitudes.

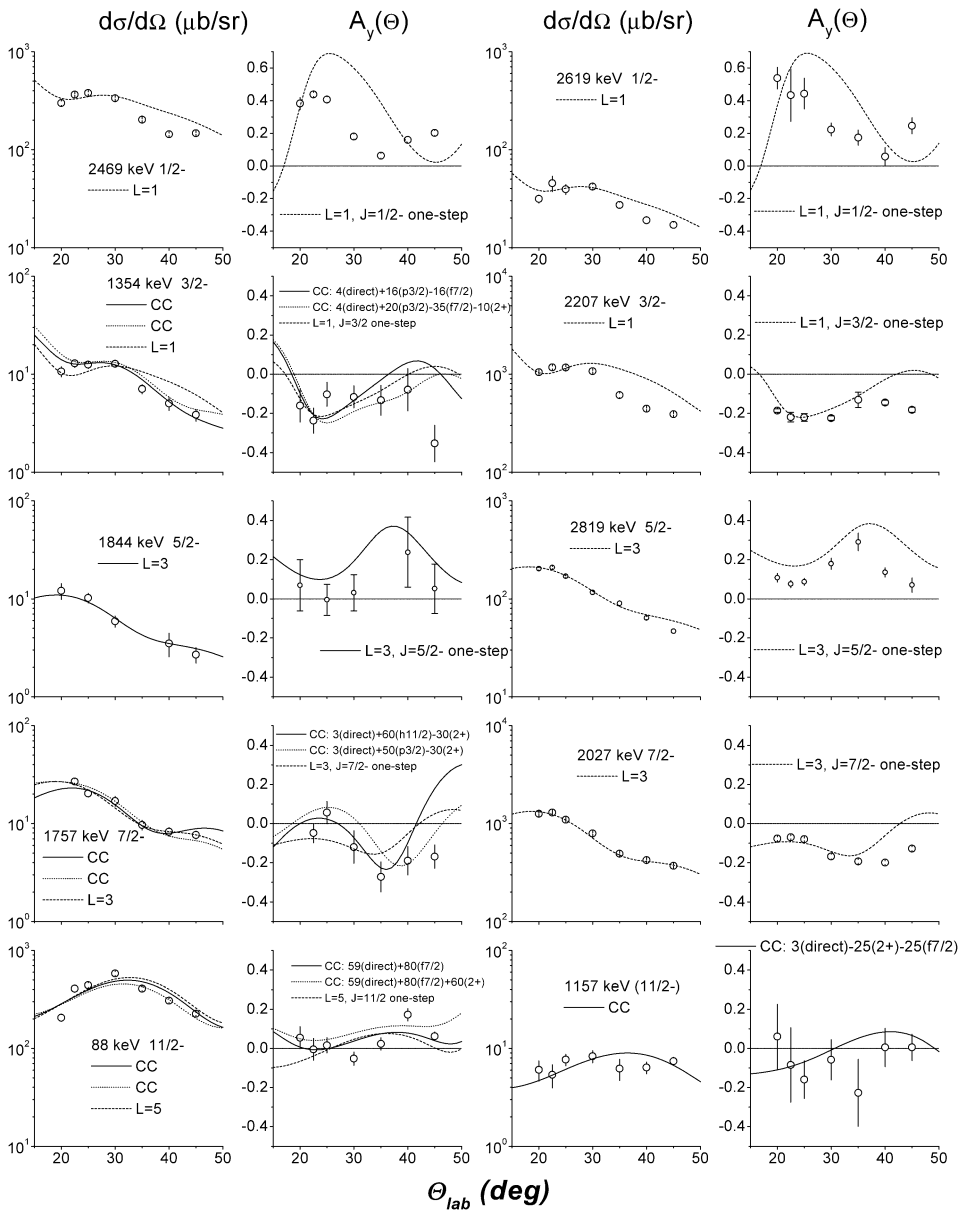

Fig. 4. The same as Fig. 3 but for negative-parity levels.

gates. Energies and intensities of the γ-rays listed in Table 1 were used for the level energies determination by a least-squares fit procedure [37] where the recoil energy and the systematic error of the energy scale calibration were taken into account. With respect to the energy calibration of the (d, p) spectra which was done by means of level energies

determined from (n, γ) experiment final level energies included in the last but one column of Table 4 are mainly from (n, γ) measurement.

Spin-parity assignments were deduced mostly from the angular distributions of cross section and asymmetry in the (d, p) reaction. For the levels observed only in the (n, γ) reaction the J^π values are assumed to be $1/2^\pm$ or $3/2^\pm$ if they are fed by primary transitions. For the levels not populated by primary transitions additional spin-parity restrictions follow from assumption that only depopulating γ-rays of E1, M1 and E2 multipolarities could be observed. Spins of levels populated and depopulated by gamma cascades are restricted in most cases to 1/2–7/2 values. Some levels reported previously [16], namely 603 ($5/2^+$), 966 ($5/2^+$), 984 and 1176 keV, could not be confirmed since they show neither coincidence relationships of populating and depopulating γ-rays nor are they seen in the (d, p) spectra. It seems likely that the (d, t) peak at 603 keV reported by Rødland et al. [19] is a contaminant by ^{129}Te. Many other levels are confirmed but their characteristics are changed in accordance with the present more precise data. Comparing the excitation energies of the present study with values from the previous stripping reaction studies we note that all energies from the literature [16] were gradually shifted to lower energies in the region between 0.6 and 2.2 MeV due to wrong calibration. The roughly constant difference of 19 keV still remains above this energy up to 3.5 MeV. We also found that many levels above 2 MeV reported in Ref. [16] are actually multiplets.

3.2. Spectroscopic strengths

Since most spins and parities have been assigned by DWBA and CCBA analyses, the spectroscopic information reliability depends on the character of the transfer reaction in each case. The inelastic form factors are usually not known in detail and it is impossible to get an exhaustive analysis. The complexity of the analysis within multi-step routes rises quickly especially for weakly excited states. As mentioned in Section 2.3 the evidence for inelastic contributions is found even in the neutron transfer to the lowest excited states including the ground state. Accounting for possible CC contributions to the ground and first excited states, the spectroscopic strengths of the direct transfer is reduced by about 25% compared to the previous published values in Ref. [16].

Only three $l = 0$ transitions are firmly established in the present study instead of at least six $1/2^+$ states reported in Ref. [16]. Other possible $1/2^+$ states at 1889 and 2120 keV are not observed in the (d, p) reaction but others at 1956, 2010 and 2458 keV do not belong to this category. Thus the experimental summed $l = 0$ strength does not exceed $S_{lj} = 0.25$.

The $l = 2$ transitions mainly result from the population of hole states in the $2d_{3/2}$ and $2d_{5/2}$ shell. Measuring asymmetries is helpful in distinguishing between two categories of $l \pm 1/2$ states, thus the strength analysis is possible for both sets separately.

We observed eight $3/2^+$ states already below 2 MeV. For the first four states we are able to fit the experimental angular distributions reasonably well by the DWBA. The behavior of the angular distributions of asymmetry is changing from one state to the other which needs special fits by inclusion of several CC routes with different 3s, 2d and 2^+ amplitudes. The last four states together with others above 2 MeV are weakly populated and the insufficient accuracy of angular patterns does not allow the DWBA analysis. As an exception two states

at 2730 and 2759 keV are well described by CCBA. Also the 2767 keV level permits the $3/2^+$ assignment.

Previous information about $5/2^+$ states comes merely from pick-up studies [19]. In the present work seven $5/2^+$ states were firmly established. The angular distributions of all states can be rather well reproduced by DWBA. At the same time as in the case of $3/2^+$ states the fitting of the angular distributions of asymmetry demands the inclusion of additional inelastic routes. However, the cross section and asymmetry of the first $5/2^+$ state at 473 keV cannot be reproduced properly by CCBA. The poor reproduction is probably due to its almost pure collective nature because of the very low cross section. The (d, p) peak corresponding to the level at 783 is overshadowed by the dominating $l = 3$ transfer to the 786 keV state. The $5/2^+$ assignment is also possible for the remaining levels at 1602, 1683 and 1704 keV. Their yield should not seriously affect the sum rule value.

Levels populated by $l = 4$ transitions stem mainly from the population of hole states in the $1g_{7/2}$ shell. For eleven states observed previously in pick-up studies [19] $7/2^+$ assignments were mostly proposed. The corresponding transfer in the (d, p) reaction is expected to be weak. We observed eight peaks but only for the three lowest states the angular information is sufficient to assign j-values. Again, while the angular distributions permit a reasonable reproduction by DWBA calculations the analyzing powers deviate very strongly from the pure direct pattern. The A_y distribution of the first $7/2^+$ at 685 was found to be well described as mainly inelastic transfer through the 2^+ state in the target channel together with the excitation in the final channel through the ground state assuming $2d_{3/2}$. The amplitude ratio of both routes is close to 50/50. For the second $7/2^+$ at 924 keV the same ratio could be even 80/50 (see Fig. 3) in favor to the ground state which is too big in comparison with the population of the ground state alone. The shapes of both $\sigma(\Theta)$ and A_y for the third $7/2^+$ state at 1428 keV show a resemblance with the first $7/2^+$ state. For the remaining levels we have assumed a $7/2^+$ assignment since they were also observed in thermal neutron capture.

A lot of $l = 1$ transitions were established in the present study. Most of the $l = 1$ strengths is due to particle states in the $3p_{3/2}$ and $3p_{1/2}$ shells. Nevertheless, several low $3/2^-$ states can be attributed to the coupling with $2f_{7/2}$ and even $1h_{11/2}$ orbitals. Comparing the experimental data points with the DWBA shapes several discrepancies were observed. Firstly, the second maximum in the diffractive structure is systematically shifted by 5–7° to the forward angles and a curvature of its shape is opposite to the calculated one at $\Theta \geqslant 30°$. Analyzing powers in all cases are negative for all measured angles in accordance with the DWBA calculations but often as for many other l transitions the observed values are more shifted at backward angles. The same picture was observed in a parallel study of ^{130}Te(d, p) at $E_d = 18$ MeV [13] and probably could be due to the use of optical potentials or to numerous coupled channel residuals. In spite of all difficulties the j-values were uniquely determined.

For the two lowest $3/2^-$ states at 1354 and 1687 keV the angular and A_y distributions account for at least two inelastic routes via $3p_{3/2}$ and $2f_{7/2}$ configurations with an amplitude ratio 8/16 or 16/16 (see Fig. 4). A good fit to the experimental data could be also obtained if we include the inelastic route in the target channel through the first 2^+. In this case amplitude ratios of $3p_{3/2}$, $2f_{7/2}$ and 2^+ are changed to 20/35/10 while the direct transfer contribution practically remains the same as given in Table 4. Most others $3/2^-$

states were identified unambiguously and the corresponding one-step spectroscopic factors are determined. There are some ambiguities of J^π assignments for the levels at 2494 and 2562 keV. For the former one this could be due to a close doublet structure. For the latter one the neutron capture data permit $1/2^-$ or $3/2$ assignment while the (d, p) data are better consistent with the $5/2^+$ assignment taking into account the shape of the A_y distribution. Assuming one level structure compromise could be achieved if we suppose a $3/2^-$ characteristic.

More conclusive is the comparison of experimental patterns for the $1/2^-$ states. In this case large A_y of about 0.4 at $\Theta = 25°$ is reversed compared to $3/2^-$ and could be compatible only with the shape of the one-step $l = 0$ transfer. We have established six $1/2^-$ states for which with the exception of the level at 2843 keV the shapes of $\sigma(\Theta)$ and A_y were well fitted by rather pure one-step transitions slightly influenced by small inelastic residual effects.

About two dozens of $l = 3$ transitions were found up to 3 MeV excitation energy which comprise mostly the particle states from $2f_{7/2}$ and $2f_{5/2}$ shells. The shape of differential cross sections for $l = 3$ and $l = 2$ transfer in most cases is very similar. Also the A_y distributions are not distinctive. Therefore, even the simultaneous analysis of both observable shapes is not decisive in many cases especially at higher energies. In general, the cross section magnitude stands high in our favor for the determination of the l-value. An additional criterion was that most $7/2^-$ states with the exception of few with low energy have not been observed in thermal neutron capture.

For the first six $7/2^-$ states below 2 MeV with exception two states at 786 and 1918 keV we found that the multi-step contributions are comparable with the direct component. The fitting analysis of the weakest peak at 1757 keV shows that the amplitude of the direct transfer is only 3 while the typical inelastic route via 2^+ gains 30. The best χ^2 fit was obtained by combining these two routes with two additional indirect routes via $1h_{11/2}$ and $3p_{3/2}$ configurations with a ratio 60/50. The importance of indirect processes is evidenced even in stronger $l = 3$ transitions mainly from the A_y shapes at $\Theta \geqslant 35°$.

The analysis of experimental patterns for the $5/2^-$ states is less conclusive since the angular information is scarce. Most j-assignments were based on the positive sign of A_y distributions with a peaking near $\Theta = 37°$. Almost identical behavior of asymmetry but with peaking at $\Theta = 28°$ takes place for $3/2^+$ states which makes this analysis rather tentative. For some states the ambiguity was resolved if the level was populated by a primary transition in thermal neutron capture.

A strong $l = 5$ transition to the $11/2^-$ state at 88 keV was observed in the (d, p) reaction. The extracted spectroscopic strength of the direct transfer from the $\sigma(\Theta)$ data is in good agreement with the previous published value in Ref. [16]. Again the analyzing power does not show a pure one-step transfer indicating a more complicated wave function structure. The $9/2^-$ states were systematically observed not far from the first $11/2^-$ state in all odd Te isotopes. These states weakly populated in nucleon transfer reaction have already been discussed in several publications [38,39] and could be attributed to the $1h_{11/2}$ family of states. The flat angular distribution of the state at 341 keV and the almost zero analyzing power established in the present study are completely determined by inelastic transfer routes. Similar pattern of both $\sigma(\Theta)$ and A_y was observed for the state at 1157 keV. Due to large ambiguities of the CCBA analysis no spins can be firmly assigned.

This state could probably be identified with the $11/2^-$ state of pick-up studies [19] but it is not the 1154 keV level observed in the (n, γ) reaction and in β-decay [16].

Table 4 collects all levels identified almost up to 3.7 MeV. Part of the observed (d, p) cross section could not be analyzed completely because of its angular uncertainty, poor statistics or unresolved multiplet structures. In Fig. 2 it is seen that the unresolved part starts at about 3.2 MeV due to the increasing density of levels. The main part of resolved peaks with certain l-assignments account for 93% of the observed total cross section. The analysis of the integrated cross sections was performed at $\Theta = 20^\circ$ where the peaking intensity takes place for most of the $l = 1, 2$ and 3 transitions. Thus, the completeness and uncertainties of the single particle strength in this energy interval are mainly limited by the accuracy of the CCBA analysis.

4. Theoretical interpretation

Our recent experimental studies of the Te nuclei in the $A \cong 130$ mass region have added rather rich spectroscopical information on low-spin structures in a broad energy interval at least up to 4 MeV. An inspection of the experimental spectra in the Te region shows a very smooth energy behavior of the levels. Since in the light odd Te nuclei ($A \leqslant 123$) the occurrence of the specific intruder states is evidenced as a consequence of the developing deformation and because these nuclei have already been discussed in detail in Ref. [1] we restrict here our analysis to the heavier group ($A = 125$–131). The systematic variations in the level energies shown in Figs. 5, 6 elucidate the filling of the valence single particle orbitals and their coupling to the adjacent even–even core. The lines connecting the levels in Figs. 5 and 6 serve firstly to show the correspondence of their experimental spectroscopic strengths. So these systematics could be considered as an extension of previous ones of Ref. [1] to the $N = 82$ shell closure. The behavior of the ^{127}Te levels in connection with theoretical model calculations will be discussed below together with the examination of their decay modes and spectroscopic strengths. The individual level description in ^{129,131}Te is discussed in detail in separate publications [12,13].

4.1. The interacting boson–fermion model

We use here like in the previous publications [1,4,6,9] the IBFM-1 version of the interacting boson–fermion model [14] which does not distinguish between neutrons and protons. Possible shortcomings of this approach related to the fact that the proton–neutron as well as the possible octupole degrees of freedom of the core are not explicitly included are compensated by the fact of its relative simplicity and reliability at low excitation energies. Thus the main features of the fragmentation of the single particle states are accounted for.

Model expressions as well as the procedure of describing the even–even core nuclei with masses from 120 to 130 with IBM-1 and the resulting parameters together with the interaction of the odd particle (fermion) with the boson core are presented in detail in [1] and we do not repeat here this general approach. The quasiparticle energies and shell occupancies have been obtained with a BCS calculation where the spherical single par-

Table 5
Experimental and theoretical electromagnetic properties of ^{127}Te states. The IBFM and QPM branchings have been calculated with the experimental level energies. Only branchings with at least one value larger than 0.1% are presented

E_x (keV)	J_i	E_f (keV)	J_f	E_γ (keV)	Exp.	IBFM	QPM
			Positive parity states				
473	$5/2_1$	0	$3/2_1$	473	100	100	49
		61	$1/2_1$	412	17	14	100
502	$3/2_2$	0	$3/2_1$	502	100	100	25
		61	$1/2_1$	441	49	49	100
623	$1/2_2$	0	$3/2_1$	623	100	100	100
		61	$1/2_1$	562	50	26	–
685	$7/2_1$	0	$3/2_1$	685	100	100	100
		473	$5/2_1$	212	12	1	–
763	$3/2_3$	0	$3/2_1$	763	100	100	100
		61	$1/2_1$	701	42	55	16
		473	$5/2_1$	289	9	28	–
		502	$3/2_2$	261	4	21	–
783	$5/2_2$	0	$3/2_1$	783	100	100	100
		61	$1/2_1$	721	15	49	16
		473	$5/2_1$	309	2	43	–
		502	$3/2_2$	281	3	52	–
924	$7/2_2$	0	$3/2_1$	924	100	100	100
		473	$5/2_1$	451	66	4	–
1075	$3/2_4$	0	$3/2_1$	1075	31	14	22
		61	$1/2_1$	1014	75	2	100
		473	$5/2_1$	602	100	100	3
		502	$3/2_2$	573	34	25	–
		623	$1/2_2$	452	29	1	–
1140	$5/2_3$	0	$3/2_1$	1140	38	33	18
		473	$5/2_1$	666	28	59	15
		502	$3/2_2$	638	86	100	–
		623	$1/2_2$	517	100	34	–
		685	$7/2_1$	454	7	–	–
		783	$5/2_2$	357	9	36	–
1309	$3/2_5$	0	$3/2_1$	1309	100	14	8
		61	$1/2_1$	1248	36	4	29
		623	$1/2_2$	686	27	10	100
		763	$3/2_3$	547	11	2	8
1405	$1/2_3$	61	$1/2_1$	1345	100	24	–
		473	$5/2_1$	932	4	14	3
		502	$3/2_2$	904	26	100	–
			Negative parity states				
631	$7/2_1$	88	$11/2_1$	543	100	68	100
		341	$9/2_1$	291	55	100	–
786	$7/2_2$	88	$11/2_1$	698	89	100	11
		341	$9/2_1$	445	100	100	79
		631	$7/2_1$	154	3	1	100
1157	$11/2_2$	88	$11/2_1$	1069	–	82	100
		341	$9/2_1$	817	100	100	–
1183	$5/2_1$	341	$9/2_1$	842	92	35	100

(*continued on next page*)

Table 5 (*continued*)

E_x (keV)	J_i	E_f (keV)	J_f	E_γ (keV)	Exp.	IBFM	QPM
		631	$7/2_1$	552	92	17	–
		786	$7/2_2$	397	100	100	–
1354	$3/2_1$	631	$7/2_1$	723	100	100	100
		786	$7/2_2$	568	10	0.3	–
		1183	$5/2_1$	171	4	18	100

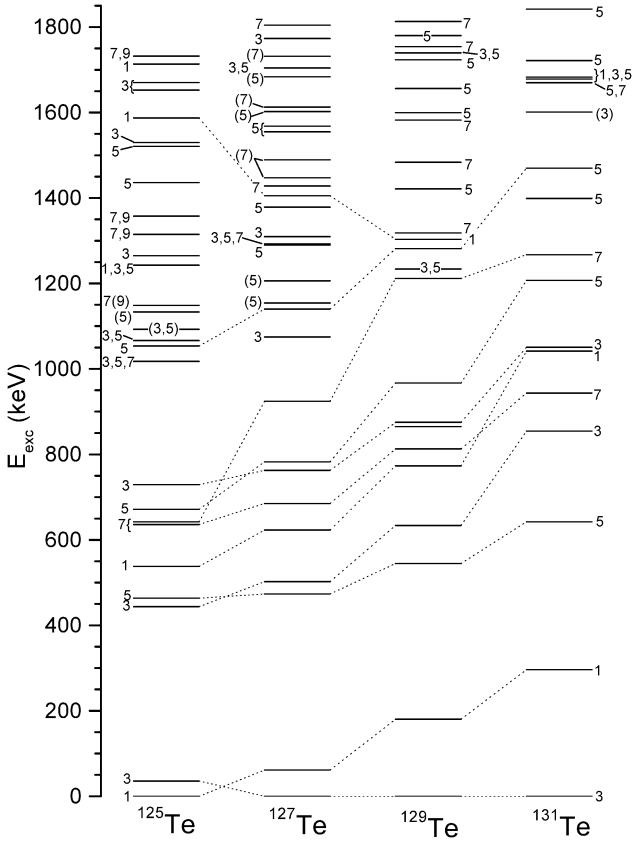

Fig. 5. Systematics of experimental positive-parity levels in the heavy odd-mass Te nuclei. Double spin values are given.

ticle orbitals between the $N = 50$ and 82 were taken from Reehal and Sorensen [40]. For the positive-parity states the odd fermion was allowed to occupy the valence orbitals $3s_{1/2}$, $2d_{3/2}$, $2d_{5/2}$ and $1g_{7/2}$. For the negative-parity states, besides the $1h_{11/2}$ unique parity orbital we have taken into account the $1f_{5/2}$, $2p_{1/2}$ and $2p_{3/2}$ 'hole' orbitals and the 'particle' orbital $1h_{9/2}$, $2f_{7/2}$, $3p_{3/2}$, $3p_{1/2}$ separately for technical reasons. The distant orbitals have been added at relative energies with respect to the $2d_{5/2}$ orbital using the universal Woods–Saxon potential of Nazarewicz et al. [41]. This provides slightly dif-

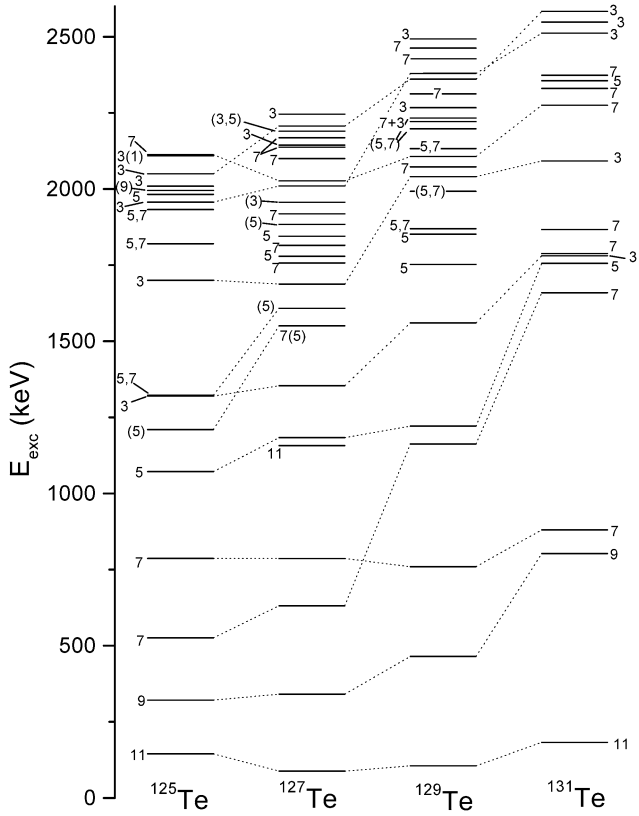

Fig. 6. The same as Fig. 5 for negative-parity levels.

ferent level energies, but the influence of the distant orbitals on the one-nucleon transfer spectroscopic strengths below 2–3 MeV is small. The actual calculations were performed with the standard programs ODDA and SPEC [42]. The boson–fermion interaction parameters used in the calculations are $\Gamma_0 = 0.2$ MeV (quadrupole–quadrupole strength) and $\Lambda_0 = 0.95$ MeV^2 (exchange strength) and $A_0 = -0.24$ MeV (monopole strength). The above Γ_0 and Λ_0 are common to the whole $^{119-129}$Te chain whereas the strength of the monopole interaction is varied almost linearly and its main effect is an overall scaling of the energy spectrum.

The results of the IBFM calculations for ^{127}Te are presented in several figures. Fig. 7 gives the general understanding of the wave-function composition for the lowest positive-parity states. Figs. 8 and 9 show a comparison between the experimental and calculated level schemes. The identification between experimental and theoretical levels in these figures is primarily based on the (d, p) spectroscopic strengths. The experimental spectroscopic strengths are compared with theoretical predictions in Fig. 10.

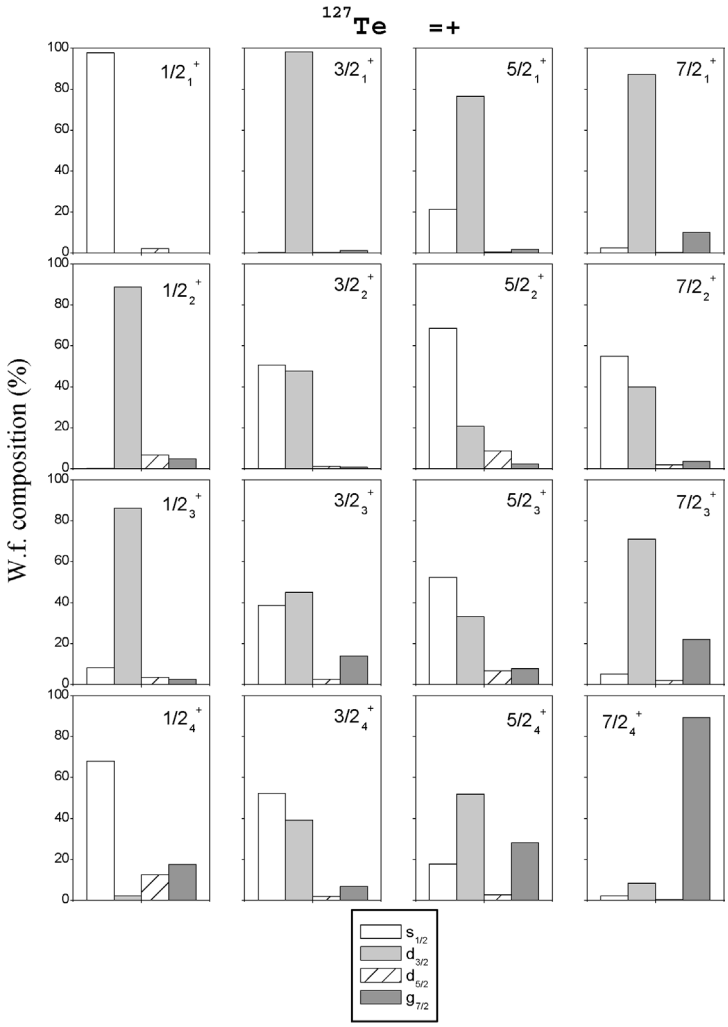

Fig. 7. The composition of the IBFM wave functions for the four lowest positive-parity states of each category in ^{127}Te.

4.2. The quasiparticle-phonon model

As known the quasiparticle phonon model (QPM) was already successful in describing collective properties in many even–even mass nuclei [15]. For odd-mass nuclei, this model was used to describe the fragmentation of deep-lying hole and high-lying particle states [43,44] and the photo-production of isomers [45–47]. A Woods–Saxon potential is used in the QPM as an average field for protons and neutrons. Phonons of different multipolarities and parities are obtained by solving the QRPA equations with residual interaction in a separable form with a Bohr–Mottelson form factor. The single-particle spectrum and phonon basis are fixed from calculations in the neighboring even–even nuclear core, i.e., in ^{126}Te.

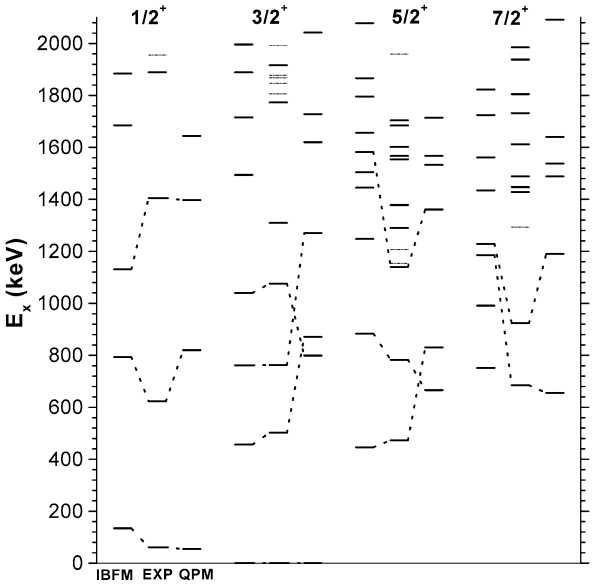

Fig. 8. Comparison of the experimental level energies with theoretical predictions for positive-parity states in ^{127}Te.

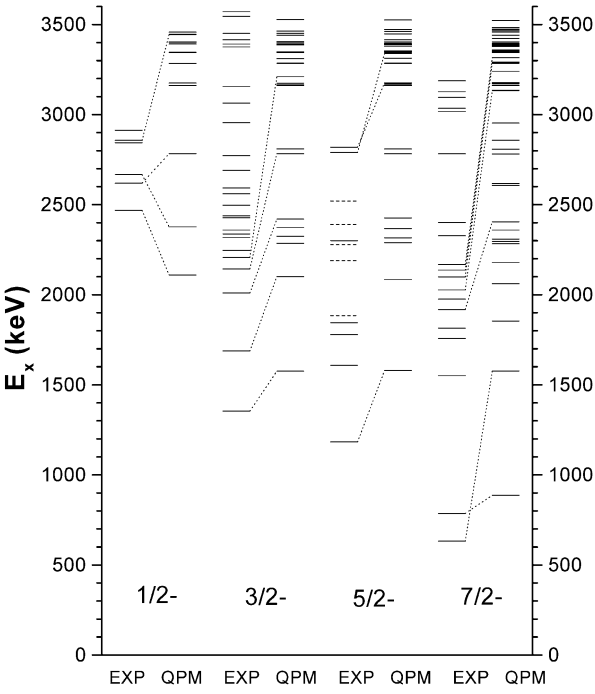

Fig. 9. Comparison of the experimental level energies with theoretical predictions for negative-parity states in ^{127}Te.

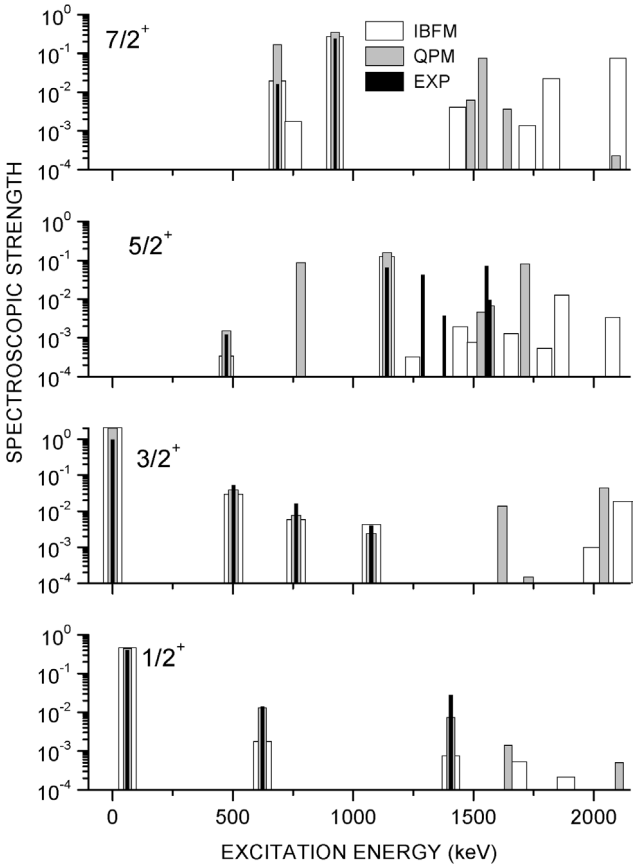

Fig. 10. Comparison of the experimental strengths $(2J+1)S_{lj}$ with theoretical predictions for positive-parity states in ^{127}Te. In accordance with the identification in Fig. 8 some theoretical strengths are plotted at the experimental level energies.

In our present calculations the wave functions of the ground state and the excited states are mixtures of different "quasiparticle $\otimes$ N-phonon" ($[qp \otimes Nph]$) configurations, where $N = 0$, 1, and 2:

$$\Psi^{\nu}(JM) = \Bigg\{ C^{\nu}(J)\alpha^{+}_{JM} + \sum_{j\beta_1} S^{\nu}_{j\beta_1}(J)\big[\alpha^{+}_{j} Q^{+}_{\beta_1}\big]_{JM} + \sum_{j\beta_1\beta_2} \frac{D^{\nu}_{j\beta_1\beta_2}(J)[\alpha^{+}_{j} Q^{+}_{\beta_1} Q^{+}_{\beta_2}]_{JM}}{\sqrt{1+\delta_{\beta_1\beta_2}}} \Bigg\} |\rangle_{g.s.} \tag{3}$$

where the coefficients C, S, and D describe a contribution of each configuration to a norm of the wave function. We use the following notations α^{+} and Q^{+} for the coupling between the creation operators of quasiparticles and phonons:

$$\left[\alpha_j^+ Q_{\lambda i}^+\right]_{JM} = \sum_{m\mu} C^{JM}_{jm\lambda\mu}\alpha_{jm}^+ Q_{\lambda\mu i}^+,$$

where C are Clebsch–Gordon coefficients. Quasiparticles are characterized by their shell quantum numbers $jm \equiv |nljm\rangle$ with a semi-integer value of the total angular momenta j. The quasiparticle energy spectrum and the occupation number coefficients u_j and v_j are obtained in the QPM by solving the BCS equations separately for neutrons and protons.

Phonons with quantum numbers $\beta \equiv |\lambda\mu i\rangle$ are linear superpositions of two-quasiparticle configurations:

$$Q_{\lambda\mu i}^+ = \frac{1}{2}\sum_{\tau}^{n,p}\sum_{jj'}\left\{\psi_{jj'}^{\lambda i}\left[\alpha_j^+\alpha_{j'}^+\right]_{\lambda\mu} - (-1)^{\lambda-\mu}\varphi_{jj'}^{\lambda i}\left[\alpha_{j'}\alpha_j\right]_{\lambda-\mu}\right\}. \tag{4}$$

A spectrum of phonon excitations is obtained by solving the RPA equations for each multipolarity λ which is an integer value. The RPA equations also yield forward (backward) $\psi_{jj'}^{\lambda i}$ ($\varphi_{jj'}^{\lambda i}$) amplitudes in the definition (4):

$$\begin{pmatrix}\psi\\ \varphi\end{pmatrix}_{jj'}^{\lambda i}(\tau) = \frac{1}{\sqrt{\mathcal{Y}_\tau^{\lambda i}}}\cdot\frac{f_{jj'}^{\lambda}(\tau)(u_j v_{j'} + u_{j'} v_j)}{\varepsilon_j + \varepsilon_{j'} \mp \omega_{\lambda i}}, \tag{5}$$

where ε_j is a quasiparticle energy, $\omega_{\lambda i}$ is the energy needed for the excitation of an one-phonon configuration, $f_{jj'}^{\lambda}$ is a reduced single-particle matrix element of residual forces, and the value $\mathcal{Y}_\tau^{\lambda i}$ is determined from a normalization condition for the phonon operators:

$$\left\langle\left|\left[Q_{\lambda\mu i}\, Q_{\lambda\mu i}^+\right]\right|\right\rangle_{ph} = \sum_{\tau}^{n,p}\sum_{jj'}\left\{\left(\psi_{jj'}^{\lambda i}\right)^2 - \left(\varphi_{jj'}^{\lambda i}\right)^2\right\} = 1. \tag{6}$$

The phonon index i is used to distinguish between phonon excitations with the same multipolarity but with different energy and structure. The RPA equations yield both, collective- (e.g., 2_1^+ and 3_1^-), and weakly-collective phonons. The latter correspond to phonons for which some specific two-quasiparticle configuration is dominant in Eq. (4) while for other configurations $\psi_{jj'}^{\lambda i}, \varphi_{jj'}^{\lambda i} \approx 0$.

When the second and third terms in the wave function of Eq. (3) are considered, phonon excitations of the core couple to a quasiparticle at any level of the average field, not only at the ones with the quantum numbers J^π as for a pure quasiparticle configuration. It is only necessary that all configurations in Eq. (3) have the same total spin and parity. The excitation energies and the contribution of the different components from the configuration space to the structure of each excited state (i.e., coefficients C, S, and D in Eq. (3)) are obtained by a diagonalization of the model Hamiltonian on a set of employed wave functions. The coupling matrix elements between the different configurations in the wave functions of Eq. (3) in odd-mass nuclei are calculated on a microscopic footing, making use of the internal fermion structure of the phonons and the model Hamiltonian. For example, the interaction matrix element between the $[qp \otimes 1ph]$ and the $[qp \otimes 2ph]$ configurations has the form (see, Ref. [44]):

$$\begin{aligned}
&\left\langle [\alpha_{jm} Q_{\lambda\mu i}]_{JM} | H | \left[\alpha^+_{j'm'} \left[Q^+_{\lambda_1\mu_1 i_1} Q^+_{\lambda_2\mu_2 i_2}\right]_{IM'}\right]_{JM} \right\rangle \\
&\quad = \delta_{jj'}\delta_{\lambda I} U^{\lambda_2 i_2}_{\lambda_1 i_1}(\lambda i) - (-)^{j'+\lambda+I} 2\sqrt{(2j+1)(2I+1)} \\
&\qquad \times \left[(-)^{\lambda_1} \delta_{\lambda\lambda_1} \begin{Bmatrix} \lambda_2 & \lambda_1 & I \\ J & j & j' \end{Bmatrix} \Gamma(jj'\lambda_2 i_2) \right. \\
&\qquad \left. + (-)^{\lambda_2} \delta_{\lambda\lambda_2} \begin{Bmatrix} \lambda_1 & \lambda_2 & I \\ J & j & j' \end{Bmatrix} \Gamma(jj'\lambda_1 i_1) \right],
\end{aligned} \tag{7}$$

where H is a model Hamiltonian, $U^{\lambda_2 i_2}_{\lambda_1 i_1}(\lambda i)$ is an interaction matrix element between one- and two-phonon configurations in the neighbouring even-mass nucleus (U is a complex function of phonon amplitude ψ and φ and $f^{\lambda}_{jj'}$; its explicit form can be found in Ref. [48]) and Γ is an interaction matrix element between quasiparticle α^+_{JM} and quasiparticle-phonon $[\alpha^+_{jm} Q^+_{\lambda\mu i}]_{JM}$ configurations, it is equal to:

$$\Gamma(Jj\lambda i) = \sqrt{\frac{2\lambda+1}{2J+1}} \frac{f^{\lambda}_{jj}(u_J u_j - v_j v_J)}{\sqrt{\mathcal{Y}^{\lambda i}_{\tau}}}. \tag{8}$$

Eqs. (7), (8) are obtained by applying the exact commutation relations between the phonon and quasiparticle operators:

$$\begin{aligned}
\left[\alpha_{jm}, Q^+_{\lambda\mu i}\right]_- &= \sum_{j'm'} \psi^{\lambda i}_{jj'} C^{\lambda\mu}_{jmj'm'} \alpha^+_{j'm'}, \\
\left[\alpha^+_{jm}, Q^+_{\lambda\mu i}\right]_- &= (-1)^{\lambda-\mu} \sum_{j'm'} \varphi^{\lambda i}_{jj'} C^{\lambda-\mu}_{jmj'm'} \alpha_{j'm'}.
\end{aligned} \tag{9}$$

The exact commutation relations between the phonon operators $Q_{\lambda\mu i}$ and $Q^+_{\lambda'\mu' i'}$,

$$\begin{aligned}
&\left[Q_{\lambda\mu i}, Q^+_{\lambda'\mu' i'}\right]_- \\
&\quad = \delta_{\lambda\lambda'}\delta_{\mu\mu'}\delta_{ii'} - \sum_{\substack{jj'j_2 \\ mm'm_2}} \alpha^+_{jm}\alpha_{j'm'} \\
&\qquad \times \left\{ \psi^{\lambda i}_{j'j_2} \psi^{\lambda' i'}_{jj_2} C^{\lambda\mu}_{j'm'j_2m_2} C^{\lambda'\mu'}_{jmj_2m_2} - (-)^{\lambda+\lambda'+\mu+\mu'} \varphi^{\lambda i}_{jj_2} \varphi^{\lambda' i'}_{j'j_2} C^{\lambda-\mu}_{jmj_2m_2} C^{\lambda'-\mu'}_{j'm'j_2m_2} \right\},
\end{aligned} \tag{10}$$

are used to calculate the interaction matrix elements U in even–even nuclei.

Eq. (7) shows that an unpaired quasiparticle does not behave as a spectator but modifies the interaction between the complex configurations compared to an even-mass nucleus (see second term in this equation). This takes place because the phonons possess an internal fermion structure and the matrix elements Γ correspond to an interaction between an unpaired quasiparticle and the two-quasiparticle configurations composing the phonon operator.

In the actual calculations, the phonon basis includes the natural parity phonons with multipolarity and parity λ^π from 0^+ to 7^-. Several low-energy phonons of each multipolarity are included in the model space. The most important ones are the first collective 2^+, 3^- and 4^+ phonons. Non-collective low-lying phonons of an unnatural parity and

natural parity phonons of higher multipolarities are of a marginal importance. To make realistic calculations possible one has to truncate the configuration space. We have done this on the basis of excitation energy arguments. All $[qp \otimes 1ph]$ with $E_x \leqslant 6.5$ MeV, and $[qp \otimes 2ph]$ with $E_x \leqslant 7.5$ MeV configurations, which do not violate the Pauli principle, are included in the model space. By doing this all the important configurations for the description of low-lying states up to 4 MeV are included in the model space. The dimension of this space depends on the total spin of the excited states, and it varies between 500 and 1500 configurations.

4.3. *Positive-parity states*

Positive parity states of ^{127}Te can be populated in a (d, p) reaction predominantly via emptiness in the valence shell model orbitals $3s_{1/2}$, $2d_{5/2}$, $2d_{3/2}$ and $1g_{7/2}$ from the 50–82 major shell. At higher excitation energies one could expect particle states following from the coupling of quasiparticle from the next higher major shell to a collective degree of freedom. Due to this coupling the states of this category could drop to the lower excitation energies. Our experimental data do not give a direct evidence for these states. Based on the good agreement between the numbers of experimental levels and the prediction of the IBFM calculation, which takes into account only the valence orbitals, up to 1.8 MeV we can anticipate that such states should lie above this excitation energy.

The $1/2^+$ *states* The first $1/2^+$ state in terms of the spectroscopic strengths or the wave functions could be interpreted as a pure $3s_{1/2}$ state having a content almost 98% in IBFM and 89% in QPM. While the experimental stripping and pick-up spectroscopic factors are in a nice agreement (see Fig. 10) with both models there is also clear evidence as mentioned in preceding sections for more residuals in their structure. The second state at 623 keV weakly populated in the (d, p) and unobserved in the pick-up reaction is dominated by the $2d_{3/2}$ intrinsic single particle state with a content of 88% in IBFM and 81% in QPM. The experimental (d, p) strength agrees well with the QPM value. Contrary the IBFM gives a value one order of magnitude smaller. The experimental angular distributions of cross section and asymmetry are fitted by inclusion in the CCBA analysis of the 2^+ state in ^{126}Te and the ground state in ^{127}Te as two possible intermediate states with an amplitude ratio 40/30. The third state at 1405 keV is populated in (d, p) slightly stronger than the second one and it is also seen in the pick-up process. The shapes of the angular distributions of cross section and asymmetry of both states are very similar and could be fitted by CCBA if all three routes via 2^+, $3/2^+$ ground state and $1/2^+$ at 61 keV are taken into account. The third state predicted by the IBFM is of almost similar structure as the second state. The same state in QPM has 38% of $3s_{1/2}$ coupled with 0_1^+ phonon and 50% of the same $3s_{1/2}$ coupled with two phonons of 2_1^+ type. This QPM structure gives the spectroscopic factor nearly four times smaller than the present experimental (d, p) value and about two times smaller than the corresponding pick-up value reported in Ref. [19]. Besides these states the QPM predicts about 16 states below 3 MeV excitations with a summed (d, p) strength $(2J + 1)S = 0.564$ which could be compared with the estimated experimental maximal value of 0.5. Thus it is not surprising that the remaining $1/2^+$ states were not observed in the present study.

The $3/2^+$ *states* The first $3/2^+$ state belongs to the ground state and is assigned to the pure $2d_{3/2}$ intrinsic state with no less than 93% in IBFM as well as in QPM calculations. Again additional residuals are evidenced in the ground state. The second $3/2^+$ state at 502 keV is populated with more than one order of magnitude weaker (d, p) and (d, t) strengths. The experimental (d, p) data propose the population via at least 2^+ and $3/2^+$ ground state with a ratio 45/27. The IBFM gives a rather mixed structure 51% $3s_{1/2} + 48\%$ $2d_{3/2}$ which reasonably well reproduces the experimental stripping and pick-up strengths. On the other hand, based on the comparative spectroscopic factors the second experimental $3/2^+$ level can be assigned to the third $3/2^+$ QPM state with 65% $3s_{1/2} + 19\%$ $2d_{3/2}$. The de-excitation mode is in agreement with a more mixed case. The third $3/2^+$ state at 763 keV is populated scarcely weaker than the former state. The angular distributions of cross section and asymmetry shapes are successful in fitting mainly via the ground state and to a small degree through the $3s_{1/2}$ state at 61 keV. The gamma branching, 65% to the ground state and 27% to the level at 61 keV, is in agreement with this feature. In the IBFM calculations this state is also mixed 45% $2d_{3/2} + 39\%$ $3s_{1/2} + 14\%$ $1g_{7/2}$. This experimental level can be assigned to the second $3/2^+$ QPM state. The QPM calculations give for this state practically the same percentage as for the third calculated state but with opposite order of main amplitudes. Both calculated spectroscopic factors are in rather good agreement with the experimentally observed values. The fourth $3/2^+$ state with a very small direct transfer is populated in (d, p) mainly through the $2d_{3/2}$ ground state and $3s_{1/2}$ state at 61 keV in an amplitude ratio of about 50/40. The collective nature of this state is supported by the character of γ-decay. Among 5 transitions from this level no one has an evident preference in intensity. The IBFM structure is very similar to the preceding two states with only minor changes. In the QPM this state is largely built on the $2d_{3/2}$ quasiparticle orbital where roughly 39% $2d_{3/2} \otimes 0_1^+ + 50\%$ $2d_{3/2} \otimes [2_1^+ \otimes 2_1^+]_0$. The experimental S-factors are in nice agreement with the both model predictions.

Below 3 MeV the QPM predicts in total 24 states with characteristic $3/2^+$ among these at least one half were observed in the present work. Besides the states mentioned above there are the states at 1309, 1773, 1878, 2120, 2176, 2329, 2730, 2759 and probably 2767 keV. All these states with the exception of three last levels are weakly populated in the stripping as well as in pick-up reaction, consequently they might come from the coupling with numerous phonon configurations. The experimental (d, p) strengths for the level at 2730 and 2759 keV agree relatively well with the calculated QPM levels at 2483 and 2808 keV, their energy centroids are surprisingly assent. The summed spectroscopic (d, p) strength for the $3/2^+$ states below 3 MeV was estimated to be 1.1 which could be compared with the corresponding QPM strength of 1.7. For the calculation of the pick-up strength from Ref. [19] we have made some corrections for wrong spin assignments because most of the states were considered to have $5/2^+$. We have assumed in accordance with DWBA that the ratio of S_{lj} of the $3/2^+$ states to the $5/2^+$ is 1.65. Thus the sum of the pick-up strength is estimated to be about 2.9, whereas the QPM prediction is 2.28.

The $5/2^+$ *states* There is a group of seven firmly established $5/2^+$ states. Their spectroscopic factors can be readily compared with the two model predictions. The first $5/2^+$ state at 473 keV is one of the weakest states populated predominantly by inelastic transfer routes. This collective state can be assigned to the first IBFM state, while with respect to QPM it

is the second state. A nearly equivalent structure is provided by the coupling of $2d_{3/2}$ and $3s_{1/2}$ quasiparticles to the 2^+ one boson (phonon) with ratios 76/21 for IBFM and 69/18 for QPM, respectively. The experimentally observed stripping and pick-up strengths are in a reasonable agreement with both models predictions. The second $5/2^+$ state at 783 keV has the strongest experimental pick-up strength in this nucleus. The corresponding (d, p) intensity is obscured by the close lying stronger peak belonging to the $7/2^-$ state. Taking into account that some (d, t) intensity of Ref. [19] may belong to the $7/2^-$ level we assign the experimental $5/2_2^+$ state to the second IBFM state or to the first QPM state. In this case both models give comparable wave function structures dominated again by the $2d_{3/2}$ and $3s_{1/2}$ states. Most of remaining stripping and pick-up strengths are almost equally shared between the next four $5/2^+$ states. We note the good $(d, p)/(d, t)$ correspondence of the experimentally observed strengths. With respect to the model strengths we emphasize that the largest strength is concentrated in the sixth IBFM state, whereas the QPM gives the third state. Also the QPM predicts somewhat more mixed structures. Gamma-decay data indicate possible $1g_{7/2}$ components in the third and more conclusively in the fourth experimental level which is in accordance with the wave function structure shown in Fig. 7.

Summation of the individual (d, p) strengths of the six $5/2^+$ states, shown in Fig. 10, yields about 0.23. The corresponding summed QPM strength over 26 states below 3 MeV is 0.28. The summed experimental (d, t) strength using data from [19] is estimated to be 4.9, whereas the QPM prediction is 4.87. In general similar results were obtained from IBFM calculations. Thus we can state that the almost full collected $2d_{5/2}$ strength is concentrated at least below 2 MeV excitation and its value agrees well with both models.

The $7/2^+$ states Only two $7/2^+$ states are sizably excited in the (d, p) reaction and they can readily be assigned to the first two QPM states. The IBFM calculations predict the largest spectroscopic strength for the fourth state which can be assigned to the second experimental $7/2^+$ state at 924 keV. As was already mentioned in Section 3.2 the first two levels are populated inelastically in (d, p) mainly through the $2d_{3/2}$ ground state and the 2^+ state of the even–even core. This experimental feature is in agreement with both model predictions which treat the three lowest $7/2^+$ levels as states largely built on the $2d_{3/2}$ component in combination with the one-boson or phonon of 2^+ type. Further comparison with model predictions is made using the (d, t) data from Ref. [19] since the present (d, p) and (n, γ) information is scarce. Nevertheless, the assignments in several cases, as one can see in Fig. 8, are not straightforward, but the (d, t) sum rule agrees with the model predictions. Thus the summed value over 12 experimental levels of about 6.82 could be compared with the QPM value of 7.13 which comprise 25 calculated levels below 3 MeV.

4.4. Negative-parity states

The family of negative-parity states observed in the present study is almost complete up to 3 MeV. Consequently the relative energy positions and their individual properties are of special interest for the comparison with theoretical models. The detailed description of the properties of some light Te isotopes ($A \leqslant 125$) in the framework of IBFM-1 is already given in Refs. [1,6,9]. The overall agreement can be stated to be fairly good up to about 1.5 MeV. Above this energy the calculated total number and distributions of levels

becomes essentially smaller than the experimental one. Moving to the shell closure this feature is enhanced by the boson cut-off effect and consequently the IBFM-1 description is not adequate to the reality. Here we present the description of the level scheme in the framework of QPM only.

Fig. 9 shows a comparison between calculated and measured spectra. The first few calculated levels of each spin category easily follow the experimental levels. They can be interpreted as members of the lowest multiplet formed by the coupling of the $1h_{11/2}$ neutron quasiparticle to the 0^+, 2^+, 4^+ and 6^+ phonons. In general, the dominance of the $1h_{11/2}$ orbital remains unchanged in all first 15–17 calculated states even for the lowest spin values. While the calculated $1h_{11/2}$ strength is concentrated only in the first $11/2^-$ state (98%) the corresponding experimentally observed (d, p) strength amounts only to about 53% of the expected value. On the contrary, the experimental (d, t) strength gives good account of predicted one. This stripping-pick-up asymmetry, even more pronounced in ^{125}Te, is puzzling since the (d, p) deficit would mean that the missing part could be found at higher energies. No such states with an exception of the weakly populated level at 1157 were observed in the present work.

The $1/2^-$ *states* Six $1/2^-$ states were established below 3 MeV. The QPM predicts only three states in this region belonging to the $1h_{11/2}$ family and their strengths are one order of magnitude smaller than the observed one in the (d, p) reaction. The summed value over six states does not exceed 10% of the expected value. Comparing the $1/2^-$ level placements in ^{127}Te with ^{129}Te there is a systematic rise in energy of about 0.3 MeV thus in accordance with [12] most of the $3p_{1/2}$ strength is distributed outside the analyzed part of the spectra. The QPM predicts a large number ($\approx$120) of $1/2^-$ states mostly with negligibly small spectroscopic factors. As a consequence, they could not be seen in the one-step transfer reactions. In general, the calculated distribution of the $3p_{1/2}$ strength is rather sharp with the energy centroid at 5.7 MeV.

The $3/2^-$ *states* Twenty six $3/2^-$ states were observed in the region below 3.7 MeV, only five of them are conformed with the QPM predictions considering the resemblance of its spectroscopic factors. In Fig. 11 we summarize the observed spectroscopic factors S_{lj} in an incremental plot as a function of excitation energy. The first sharp step in the experimental distribution takes place at 2.2 MeV where five states comprise about 22% of the whole $3p_{3/2}$ strength. The next increase of the strength is indicated at 3.4 MeV and further the smooth behavior continues probably up to the 5.2 MeV. Here we have used the data from Ref. [17] (shown by the dashed line) obtained with the unpolarized deuteron beam. Therefore the sum rule analysis is not rigorous. The QPM predicts also a two-step behavior of the $3/2^-$ strength distribution, but the calculated picture is shifted to higher energies by about 1.7 MeV. Again 70% of the calculated sum rule falls on about ten states in the energy interval between 5.1 and 6 MeV.

The $5/2^-$ *states* Within the excitation energy range studied, twelve $5/2^-$ states were identified which carry together about 4% of expected total strength. This deficit of spectroscopic sum may be viewed as the tail of the $2f_{5/2}$ strength whose main part tends to lie higher. The QPM predicts the energy centroid of the $2f_{5/2}$ distributions at 6.7 MeV.

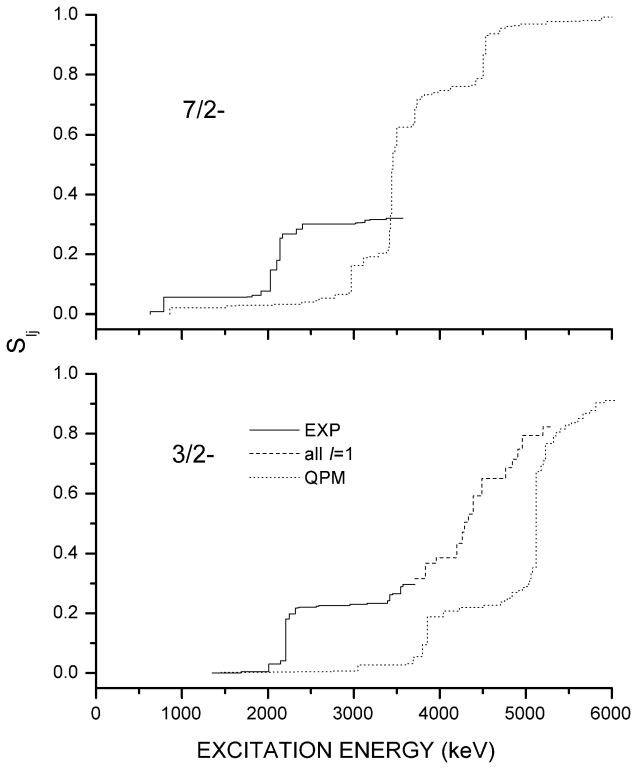

Fig. 11. The experimental and the QPM cumulative sums of spectroscopic factors S_{lj} for $3p_{3/2}$ and $2f_{7/2}$ orbitals in ^{127}Te. The dashed line represents the full experimental $l = 1$ strength above 3.7 MeV for both $1/2^-$ and $3/2^-$ states. Data were taken from Ref. [17].

The $7/2^-$ *states* In the present (d, p) study eighteen $7/2^-$ states were observed in an excitation energy range up to 3.4 MeV. The resultant cumulative yield of the $7/2^-$ strength reaches $1/3$ of the total sum rule. This is shown in Fig. 11. Like the $3p_{3/2}$ distribution the $2f_{7/2}$ strength starts to rise steeply at 2 MeV. This behavior of the $2f_{7/2}$ strength is firmly retained for the all heavy Te ($A \geqslant 125$) isotopes. Also the QPM demonstrates the same trend although the energy shift of about 1 MeV towards to high energies is clearly evidenced. The calculated $2f_{7/2}$ strength is obviously very fragmented, but a detailed comparison with the experiment is really impossible because of the incomplete spectroscopic sum. Nevertheless, the appearance of one group of $3/2^-$ and another group of $7/2^-$ states is remarkable in a rather narrow energy interval between 2.0 and 2.3 MeV. Their correlated behavior is obviously connected with the configurational mixing between $3p_{3/2}$ and $2f_{7/2}$ orbitals but the experimental details of the coupling remain unclear.

The lower group of $3/2^-$ states can be interpreted according to the QPM as the superposition of $2d_{3/2}$ quasiparticles coupled with the 3^-_{1-4} phonons and $2f_{7/2}$ quasiparticles coupled with the 2^+_1 phonon. The theory predicts 42 states below 3.8 MeV about 10 of them comprise 20% of the whole $3/2^-$ strength. The mentioned components in these ten

$3/2^-$ states vary from 8% to 70%. Similarly, the first group of experimental $7/2^-$ states around 2 MeV can be interpreted as superposition of $2d_{3/2}$ and $3s_{1/2}$ quasiparticles coupled with the 3^- phonons. In this case the QPM predicts 19 states below 3 MeV two of them consist of the 3_1^- phonons and collect 12% of the whole $7/2^-$ strength.

5. Thermal neutron capture cross section of ^{126}Te

Like in other Te isotopes the recommended value of the thermal neutron capture cross section of ^{126}Te in the BNL atlas [52] is based on very old measurements. The present (n,γ) experiments allow the determination of a new value of this cross section.

To determine this cross section we performed a supplement measurement with a composite Al–Te–Al sandwich target. Using the well known cross section of ^{27}Al and the intensity of 100% of the 1778 keV line from the β decay of ^{28}Al we evaluated the partial cross sections of the γ lines from the ^{126}Te$(n,\gamma)^{127}$Te reaction, $\sigma_{n\gamma}^{i}$. Then the total thermal neutron capture cross could be calculated via

$$\sigma_{n\gamma}^{g+m} = \frac{\sigma_{n\gamma}^{i}}{I_{\gamma}^{i}}, \tag{11}$$

where I_{γ}^{i} are the absolute γ intensities (see Section 2.1 for their determination). Evaluating Eq. (11) for the dominant 2145 keV line we arrived at the value $\sigma_{n\gamma}^{g+m} = 0.44 \pm 0.06$ b. Combining this result with the ratio of the population of the isomeric $11/2^-$ state and the ground state one can determine also the isomeric cross section to be $\sigma_{n\gamma}^{m} = 0.069 \pm 0.010$ b.

Both these values are significantly smaller than those given in the BNL neutron cross section atlas [52] ($\sigma_{n\gamma}^{g+m} = 1.04 \pm 0.15$ b and $\sigma_{n\gamma}^{m} = 0.135 \pm 0.023$ b). On the other hand, the present value of the isomeric cross section is in a very good agreement with the recently published value 0.0625 ± 0.0056 b [49]. The enhanced population of the long-lived odd Te isomers was explained in detail in Ref. [50].

Recently new values for thermal neutron capture cross sections of the tellurium isotopes were reported in Ref. [51]. The cross section for the isotope ^{126}Te, $\sigma_{n\gamma}^{g+m} = 0.55 \pm 0.06$ b, in that work is based on the same (n,γ) experiment. However, the different methods of normalization of the intensities I_{γ}^{i} and the different measurements for evaluation of the partial cross sections $\sigma_{n\gamma}^{i}$ were used in these two works. Thus the value of the thermal neutron cross section given in this subsection can be considered as an essentially independent check of our recommended value which was reported in Ref. [51].

6. Direct neutron capture

In our previous papers on ^{128}Te [12] and ^{130}Te [13] we observed the direct capture mechanism. In these nuclei the direct capture mechanism is responsible for the total thermal neutron capture. This value is for both nuclei 0.24 b [51]. However, this cross section is significantly larger for ^{126}Te, 0.55 b [51] or 0.44 b from the previous section. Assuming a similar contribution of the direct capture mechanism in all three Te isotopes, one could

Table 6
Calculation of direct capture and expected compound capture contributions for E1 transitions. See text for explanation of symbols

E_f (keV)	E_γ (keV)	J^π	$(2J_f+1)S_{dp}$	σ^{DC} (mb)	σ^{exp} (mb)	$\langle\sigma^{\mathrm{CN}}_{\mathrm{BA}}\rangle$ (mb)	$\langle\sigma^{\mathrm{CN}}_{\mathrm{KMF}}\rangle$ (mb)
1354	4934	$3/2^-$	0.0048	0.39	0.81	7.85	1.90
1687	4601	$3/2^-$	0.013	0.99		5.77	1.36
2009	4278	$3/2^-$	0.108	7.6	9.4	4.21	0.97
2144	4144	$3/2^-$	0.072	4.9	10.3	3.67	0.84
2207	4081	$3/2^-$	0.56	37.4	57.2	3.43	0.79
2246	4042	$3/2^-$	0.068	4.5	2.4	3.30	0.76
2318	3971	$3/2^-$	0.076	4.9	10.5	3.06	0.70
2469	3819	$1/2^-$	0.16	9.9	28.0	2.59	0.59
2619	3668	$1/2^-$	0.018	1.1	6.4	2.18	0.50
2667	3621	$1/2^-$	0.014	0.82	2.6	2.06	0.47
2857	3432	$1/2^-$	0.006	0.33	0.85	1.65	0.38
2955	3333	$(3/2^-)$	0.016	0.86	3.8	1.46	0.34
3392	2896	$3/2^-$	0.036	1.7	2.4	0.81	0.20
3416	2872	$3/2^-$	0.076	3.5		0.78	0.19
3545	2742	$(3/2^-)$	0.096	4.2	3.0	0.65	0.16
3572	2716	$(3/2^-)$	0.028	1.2		0.62	0.16
Sum			1.352	84.3	137.7	44.1	10.3

interpret the difference by the contribution of the compound nucleus mechanism. Thus, the reaction $^{126}\mathrm{Te}(n,\gamma)^{127}\mathrm{Te}$ represents a opportunity for the investigation of the interplay of these mechanisms.

The commonly used formula for direct capture contributions is given in the atlas of neutron cross section [52]:

$$\sigma_{\gamma f}(\text{channel}) = \sigma_{\gamma f}(\text{hard sphere})\left[1 + \frac{R - a_{\mathrm{coh}}}{R} Y_f \frac{Y_f + 2}{Y_f + 3}\right]^2, \tag{12}$$

where

$$\sigma_{\gamma f}(\text{hard sphere}) = \frac{0.062}{R\sqrt{E_n}}\left[\frac{Z}{A}\right]\frac{2J_f + 1}{6(2J_t + 1)} S_{dp} Y_f^2 \left[\frac{Y_f + 3}{Y_f + 1}\right]^2 \tag{13}$$

and

$$Y_f^2 = \frac{2m E_\gamma R^2}{\hbar^2}. \tag{14}$$

Z is the proton number, A is the atomic number, R is the interaction radius (usually taken in the form $1.35 \times A^{1/3}$ fm), a_{coh} is the coherent scattering length, J_f is the total spin of final state, J_t is the spin of the target, S_{dp} is the (d, p) spectroscopic factor, E_γ is the energy of the primary γ transition and E_n is the incident neutron energy (0.0253 eV for 2200 m/s neutrons).

The calculated contributions of direct capture σ^{DC} are compared with the experimental values of partial capture cross sections σ^{exp} in Table 6. The presence of the direct capture mechanism in the $^{126}\mathrm{Te}(n,\gamma)^{127}\mathrm{Te}$ reaction is clearly seen from this comparison. The

correlation between these two sets of 16 values is documented with the high correlation coefficient $\varrho_{\exp} = \varrho(\sigma^{\mathrm{DC}}, \sigma^{\exp}) = 0.957$. Looking at this high correlation coefficient, important questions arise, What is an influence of the compound nucleus mechanism on this correlation? Is this correlation too high regarding the significant contribution of the compound nucleus mechanism? In the following paragraphs we will address these questions.

The expectation values of the partial capture cross sections corresponding CN mechanism can be expressed as

$$\langle \sigma_{\gamma f}^{\mathrm{CN}} \rangle = \sigma_{\gamma}^{\mathrm{CN}} E_{\gamma}^{3} D S_{\gamma} / \langle \Gamma_{\gamma}^{\mathrm{CN}} \rangle, \tag{15}$$

where f denotes a final state, $\sigma_{\gamma}^{\mathrm{CN}}$ is a part the total neutron capture cross section corresponding to the CN mechanism, D is the average spacing between s-wave resonances, S_{γ} is the photon strength function for E1 transitions with energy E_{γ} and $\langle \Gamma_{\gamma}^{\mathrm{CN}} \rangle$ is the expectation value of the CN part of the total radiation width Γ_{γ}. For estimation of the CN partial contributions we assumed $\sigma_{\gamma}^{\mathrm{CN}} = \sigma_{\gamma}^{\exp} - \sum_f \sigma_{\gamma f}^{\mathrm{DC}}$ and $\langle \Gamma_{\gamma}^{\mathrm{CN}} \rangle = \Gamma_{\gamma}$, where we used the value of experimental thermal neutron cross sections $\sigma_{\gamma}^{\exp} = 0.44$ b from this work, the values $\sum_f \sigma_{\gamma f}^{\mathrm{DC}} = 0.084$ b from the Table 6 and the total radiation width were estimated from systematics of neighbouring isotopes $\Gamma_{\gamma} = 100$ meV. For S_{γ} we utilized two models, the conventional Brink–Axel (BA) giant dipole resonance (GDR) Lorentzian model [53] and the model proposed by Kadmenskij, Markushev and Furman (KMF) [54]. The estimations of expected contributions of the CN mechanism are given in the last two columns of Table 6.

Both mechanisms contribute simultaneously to the partial cross sections. The resulting partial cross section can be expressed as

$$\sigma_{\gamma f} = \left[\sqrt{\sigma_{\gamma f}^{\mathrm{DC}}} + \eta \sqrt{\langle \sigma_{\gamma f}^{\mathrm{CN}} \rangle} \right]^2, \tag{16}$$

where η takes into account Porter–Thomas fluctuation and is a realization of a random variable with the normal distribution, $f(\eta) = \frac{1}{\sqrt{2\pi}} e^{-\eta^2/2}$. Performing a Monte Carlo simulation we can test the compatibility of the experimental correlation coefficient $\varrho_{\exp} = 0.957$ with the modeled distribution of the correlation coefficients $\varrho = \varrho(\sigma_{\gamma f}, \sigma^{\mathrm{DC}})$ for $\sigma_{\gamma f}$ simulated according to Eq. (16). For two sets of $\langle \sigma_{\gamma f}^{\mathrm{CN}} \rangle$ corresponding to the Brink–Axel model and Kadmenskij et al. model of E1 PSF we obtained the expectation value of ϱ to be $\langle \varrho \rangle^{\mathrm{BA}} = 0.824$ and $\langle \varrho \rangle^{\mathrm{KMF}} = 0.966$. The probabilities for the occurrence of $\varrho > \varrho_{\exp}$ are also high, $P(\varrho > \varrho_{\exp})^{\mathrm{BA}} = 0.29$ and $P(\varrho > \varrho_{\exp})^{\mathrm{KMF}} = 0.76$. These numbers shows that our observed correlation coefficient $\varrho_{\exp}$ is not in contradiction with generally accepted ideas about the CN mechanism.

7. Conclusions

The present work represents a detailed study of the nuclear structure of ^{127}Te. The two experimental methods complement each other in their spin and energy ranges. The γ-ray and particle spectroscopy with high energy resolution in combination with polarized deuteron beams allowed the observation of about 190 levels up to 4.1 MeV. Spin-parities

and single particle strengths were assigned to the most of the observed states by using the DWBA and CCBA analyses.

The almost complete experimental set of level energies, secondary gamma-ray branches and spectroscopic strengths has been interpreted in terms of IBFM-1 and QPM calculations. Both models give a generally good description of the observable features below 2 MeV excitation energies. At higher energies, the description of the strength functions and of the degree of fragmentation of the particle-type states with the IBFM-1 becomes worse due to the boson space cut-off effect. In this respect the QPM ensures a much wider model space where its dimension varies between 500–700 configurations. A reasonably good description of the summed $3/2^-$ and $7/2^-$ strengths was obtained with the QPM. Strong correlation in their behavior at $A \cong 130$ could be recognized through the coupling interference of $2d_{3/2}$ and $3s_{1/2}$ quasiparticles to the 3^- type phonons and with the coupling of 2^+ types phonons to the $3p_{3/2}$ and $2f_{7/2}$ quasiparticles.

The transfer study reveals a series of states with 'anomalous' angular distribution of cross section and asymmetry. This could be accounted for by inelastic multi-step mechanisms. It was demonstrated that conclusions on single particle spectroscopic factors especially for the high-lying states depend crucially on the choice of proper coupled channels. Another source of uncertainties are the restricted knowledge of real form factors for the inelastic scattering interaction, the relative importance of different multipolarities in inelastic routes and to a small degree the DWBA optics that could lead to large deviations of measured distributions for individual states.

The role of the direct mechanism in thermal neutron capture on the ^{126}Te target was investigated. Unlike thermal neutron capture on the neighbouring even isotopes ^{128}Te and ^{130}Te, the compound nucleus mechanism contribute significantly to the total thermal neutron capture cross section on ^{126}Te. However, this contributions does not blur the high degree of the correlation between the (d, p) spectroscopic factors and the (n, γ) primary intensities. The new value of the thermal neutron capture cross section for ^{126}Te recently published in Ref. [51] was confirmed in this work.

Acknowledgements

The authors want to thank the Deutsche Forschungsgemeinschaft, Bonn (Eg 25/4), for generous support during working stages at the Technical University of Munich. The work has been supported by funds of the Munich Maier Leibnitz Laboratory and the Deutsche Forschungsgemeinschaft (Grant IIC4 Gr 894/2-3). Financial support has been also received from the Grant Agency of the Czech Republic (Nos. 202/03/0891, 202/99/D087) and from Ministry of Education, Youth and Sports (No. 2672244501). V.Yu.P. acknowledges support by the DFG under contract SFB 634. We are grateful to P. Maier-Komor and to K. Nacke for the target preparation and to T. Faestermann for the Q3D maintenance. The technical staff of the reactor at Řež and of the accelerator laboratory in Munich deserves appreciation for providing us with excellent beams. One of us (V.B.) is grateful also to the NPI, Řež, for the hospitality and helpful co-operation and discussions.

References

[1] D. Bucurescu, T. von Egidy, H.-F. Wirth, N. Mărginean, U. Köster, W. Schauer, I. Tomandl, G. Graw, A. Metz, R. Hertenberger, Nucl. Phys. A 672 (2000) 21.
[2] H. Dias, L. Losano, Phys. Rev. C 50 (1994) 1377.
[3] J. Jolie, K. Heyde, P. van Isacker, A. Frank, Nucl. Phys. A 466 (1987) 1.
[4] D. Bucurescu, T. von Egidy, H.-F. Wirth, N. Mărginean, U. Köster, G. Graw, A. Metz, R. Hertenberger, Y. Eisermann, Nucl. Phys. A 674 (2000) 11.
[5] W. Schauer, C. Doll, T. von Egidy, R. Georgii, J. Ott, H.-F. Wirth, A. Gollwitzer, G. Graw, R. Hertenberger, B. Valnion, M. Grinberg, Ch. Stoyanov, Nucl. Phys. A 652 (1999) 339.
[6] V. Bondarenko, T. von Egidy, J. Honzátko, I. Tomandl, D. Bucurescu, N. Mărginean, J. Ott, W. Schauer, H.-F. Wirth, C. Doll, Nucl. Phys. A 673 (2000) 85.
[7] R. Georgii, T. von Egidy, J. Klora, H. Lindner, U. Mayerhofer, J. Ott, W. Schauer, P. von Neumann-Cosel, A. Richter, C. Schlegel, R. Schulz, V.A. Khitrov, A.M. Sukhovoj, A.V. Vojnov, J. Berzins, V. Bondarenko, P. Prokofjevs, L.J. Simonova, M. Grinberg, Ch. Stoyanov, Nucl. Phys. A 592 (1995) 307.
[8] C. Doll, H. Lehmann, H.G. Börner, T. von Egidy, Nucl. Phys. A 672 (2000) 3.
[9] J. Honzátko, I. Tomandl, V. Bondarenko, D. Bucurescu, T. von Egidy, J. Ott, W. Schauer, H.-F. Wirth, C. Doll, A. Gollwitzer, G. Graw, R. Hertenberger, B. Valnion, Nucl. Phys. A 645 (1999) 331.
[10] J. Ott, C. Doll, T. von Egidy, R. Georgii, M. Grinberg, W. Schauer, R. Schwengner, H.-F. Wirth, Nucl. Phys. A 625 (1997) 598.
[11] T. von Egidy, C. Doll, J. Jolie, N.V. Warr, J. Kern, M. Crittin, L. Genilloud, Nucl. Phys. A 714 (2003) 355.
[12] H.-F. Wirth, T. von Egidy, I. Tomandl, J. Honzátko, D. Bucurescu, N. Mărginean, V.Yu. Ponomarev, R. Hertenberger, Y. Eisermann, G. Graw, Nucl. Phys. A 716 (2003) 3.
[13] I. Tomandl, T. von Egidy, J. Honzátko, V. Bondarenko, H.-F. Wirth, D. Bucurescu, V.Yu. Ponomarev, G. Graw, R. Hertenberger, Y. Eisermann, S. Raman, Nucl. Phys. A 717 (2003) 149.
[14] F. Iachello, O. Scholten, Phys. Rev. Lett. 43 (1979) 679.
[15] V.G. Soloviev, Theory of Atomic Nuclei: Quasiparticles and Phonons, Institute of Physics, Bristol, 1992.
[16] K. Kitao, M. Oshima, Nucl. Data Sheets 77 (1996) 1.
[17] A. Graue, E. Hvidsten, J.R. Lien, G. Sandvik, W.H. Moore, Nucl. Phys. A 120 (1968) 493.
[18] M.A. Shahabuddin, J.A. Kuehner, A.A. Pilt, Phys. Rev. C 23 (1981) 64.
[19] T. Rødland, J.R. Lien, G. Løvhøiden, J.S. Vaagen, V. Oygaard, C. Ellegaard, Phys. Scr. 32 (1985) 201.
[20] J. Honzátko, K. Konečný, I. Tomandl, J. Vacík, F. Bečvář, P. Cejnar, Nucl. Instrum. Methods A 376 (1996) 434.
[21] C. van der Leun, P. de Wit, C. Alderliesten, in: T. von Egidy (Ed.), Proceedings 4th Capture Gamma-ray Spectroscopy and Related Topics, vol. 62, Institute of Physics, Bristol, 1981, p. 548.
[22] B. Krusche, K.P. Lieb, H. Daniel, T. von Egidy, G. Barreau, H.G. Börner, R. Brissot, C. Hofmeyr, R. Rascher, Nucl. Phys. A 386 (1982) 245.
[23] R.G. Helmer, P.H.M. van Assche, C. van der Leun, At. Data Nucl. Data Tables 24 (1979) 39.
[24] G.L. Molnár, Z. Révay, T. Belgya, 5th International Topical Meeting on Industrial Radiation and Radioisotope measurement Applications (IRRMA-V), Bologna, Italy, 9–14 June 2002.
[25] R.B. Firestone, S.Y.F. Chu, C.M. Baglin (Eds.), Table of Isotopes, eighth ed., Wiley, 1999, update.
[26] S.T. Boneva, E.V. Vasileva, Yu.P. Popov, A.M. Sukhovoj, V.A. Khitrov, Particles Nucl. 22 (1991) 479.
[27] I. Tomandl, Ph.D. Thesis, NPI Řež, 1997, http://omega.ujf.cas.cz/~tomandl/thesis-tom.html.
[28] G. Audi, A.H. Wapstra, C. Thibault, Nucl. Phys. A 729 (2003) 337.
[29] M.O.M.D. de Souza, R.X. Saxena, Phys. Rev. C 31 (1985) 593.
[30] P. Schiemenz, Helv. Phys. Acta 59 (1986) 620.
[31] M. Löffler, H.J. Scheerer, H. Vonach, Nucl. Instrum. Methods 111 (1973) 1.
[32] E. Zanotti, M. Bisenberger, R. Hertenberger, H. Kader, G. Graw, Nucl. Instrum. Methods A 310 (1991) 706.
[33] P.D. Kunz, University of Colorado, Computer code CHUCK3, unpublished.
[34] W.W. Daehnick, J.D. Childs, Z. Vrcelj, Phys. Rev. C 21 (1980) 2253.
[35] F.D. Becchetti Jr., G.W. Greenless, Phys. Rev. 182 (1969) 1190.
[36] S. Raman, C.H. Malarkey, W.T. Milner, C.W. Nestor Jr., P.H. Stelson, At. Nucl. Data Tables 36 (1987) 1.
[37] K. Schreckenbach, Computer program LEVFIT, ILL Grenoble.
[38] T. Rødland, J.S. Vaagen, J.R. Lien, Nucl. Phys. A 338 (1980) 13.

[39] T. Rødland, J.R. Lien, G. Løvhøiden, T.F. Thorsteinsen, J.S. Vaagen, Nucl. Phys. A 469 (1987) 407.
[40] B.S. Reehal, R.A. Sorensen, Phys. Rev. C 2 (1970) 819.
[41] W. Nazarewicz, J. Dudek, R. Bengtsson, T. Bengtsson, I. Ragnarsson, Nucl. Phys. A 345 (1985) 397.
[42] O. Scholten, Computer codes ODDA and PBEM, KVI internal report No. 252, 1982, Computer code SPEC, unpublished.
[43] A.I. Vdovin, V.V. Voronov, V.G. Soloviev, Ch. Stoyanov, Part. Nucl. 16 (1985) 245.
[44] S. Gales, Ch. Stoyanov, A.I. Vdovin, Phys. Rep. 166 (1988) 125.
[45] V.Yu. Ponomarev, A.P. Dubensky, V.P. Dubensky, E.A. Boiykova, J. Phys. G: Nucl. Part. Phys. 16 (1990) 1727.
[46] M. Huber, P. von Neumann-Cosel, A. Richter, C. Schlegel, R. Schultz, J.J. Carroll, K.N. Taylor, D.G. Richmond, T.W. Sinor, C.B. Collins, V.Yu. Ponomarev, Nucl. Phys. A 559 (1993) 253.
[47] J.J. Carroll, C.B. Collins, K. Heyde, M. Huber, P. von Neumann-Cosel, V.Yu. Ponomarev, D.G. Richmond, A. Richter, C. Schlegel, T.W. Sinor, K.N. Taylor, Phys. Rev. C 48 (1993) 2238.
[48] C.A. Bertulani, V.Yu. Ponomarev, Phys. Rep. 321 (1999) 139.
[49] V.G. Alpatov, A.V. Davydov, G.R. Kartashov, M.M. Korotkov, G.V. Kostina, P.A. Polozov, A.A. Sadovsky, Yad. Fiz. 58 (1995) 15.
[50] V. Bondarenko, J. Honzátko, I. Tomandl, D. Bucurescu, T. von Egidy, J. Ott, W. Schauer, H.-F. Wirth, C. Doll, Phys. Rev. C 60 (1999) 027302.
[51] I. Tomandl, J. Honzátko, T. von Egidy, H.-F. Wirth, T. Belgya, M. Lakatos, L. Szentmiklósi, Zs. Révay, G.L. Molnár, R.B. Firestone, V. Bondarenko, Phys. Rev. C 68 (2003) 067602.
[52] S.F. Mughbahab, M. Divideenam, N.E. Holden (Eds.), Neutron Cross Section, vol. 1, Academic Press, 1981, p. 12, part A.
[53] P. Axel, Phys. Rev. 126 (1962) 671.
[54] S.G. Kadmenskij, V.P. Markushev, V.I. Furman, Sov. J. Nucl. Phys. 37 (1983) 165.